J Infrared Milli Terahz Waves (2011) 32:1074–1122
DOI 10.1007/s10762-011-9794-5

INVITED REVIEW ARTICLE

Invited Review Article: Current State of Research on Biological Effects of Terahertz Radiation

Gerald J. Wilmink · Jessica E. Grundt

Received: 13 January 2011 / Accepted: 20 April 2011 /
Published online: 7 June 2011

Abstract Terahertz (THz) imaging and sensing technologies are increasingly being used in a host of medical, military, and security applications. For example, THz systems are now being tested at international airports for security screening purposes, at major medical centers for cancer and burn diagnosis, and at border patrol checkpoints for identification of concealed explosives, drugs, and weapons. Recent advances in THz applications have stimulated renewed interest regarding the biological effects associated with this frequency range. Biological effects studies are a valuable type of basic science research because they serve to enhance our fundamental understanding of the mechanisms that govern THz interactions with biological systems. Such studies are also important because they often times lay the foundation for the development of future applications. In addition, from a practical standpoint, THz biological effects research is also necessary for accurate health hazard evaluation, the development of empirically-based safety standards, and for the safe use of THz systems. Given the importance and timeliness of THz bioeffects data, the purpose of this review is twofold. First, to provide readers with a common reference, which contains the necessary background concepts in biophysics and THz technology, that are required to both conduct and evaluate THz biological research. Second, to provide a critical review of the scientific literature.

Keywords Terahertz · THz · Thermal effects · Microarray · Cellular effects · Gene expression · Invited review · Biological effects · Review article · Radiation

CONTENTS

G. J. Wilmink (✉) · J. E. Grundt
711th Human Performance Wing, Radio Frequency Radiation Branch, Air Force Research Laboratory, Fort Sam Houston, TX, USA
e-mail: gerald.wilmink@us.af.mil

1 Introduction

The terahertz (THz) frequency region occupies a large portion of the electromagnetic (EM) spectrum that is located between the infrared (IR) and microwave (MW) regions. The THz region is typically defined to include the frequencies ranging from 0.1 to 10 THz, where 1 THz equals 10^{12} Hz. In terms of other frequently used units, this range corresponds to the following: wavelength λ (30–3000 μm); wavenumber k (3.3–334 cm^{-1}); period τ (0.1–10 picoseconds), temperature T (4.8–478 K), and photon energy E (0.4–41 milli-electron volts) (Fig. 1).

It is important to note that the energy of THz photons is several orders of magnitude below the energy level required to ionize, or remove, valence electrons from biological molecules (typically, several eVs). Thus, "T-rays" are classified as a type of *non-ionizing* radiation. This fundamental distinction is important because nonionizing and ionizing radiation generate vastly different effects in biological structures. Perhaps, the most noteworthy difference is that only ionizing radiation particles carry enough energy to cause direct ionization effects to water and biomolecules. These direct effects are particularly harmful to biological structures because they result in the formation of highly reactive free radicals, which can cause secondary or indirect damage to other biomolecules. In contrast, nonionizing radiation does not generate free radicals in biological structures, but it can cause thermal effects that are indistinguishable from effects observed from bulk heating.

For many years, data has been scarce at THz frequencies because suitable sources were not widely available. However, a recent surge in research activity has resulted in the development of many new types of sources and components. These new THz technologies have bridged the proverbial "THz Gap," and are increasingly being integrated into a host of practical medical, military, and security applications. For instance, THz imaging and

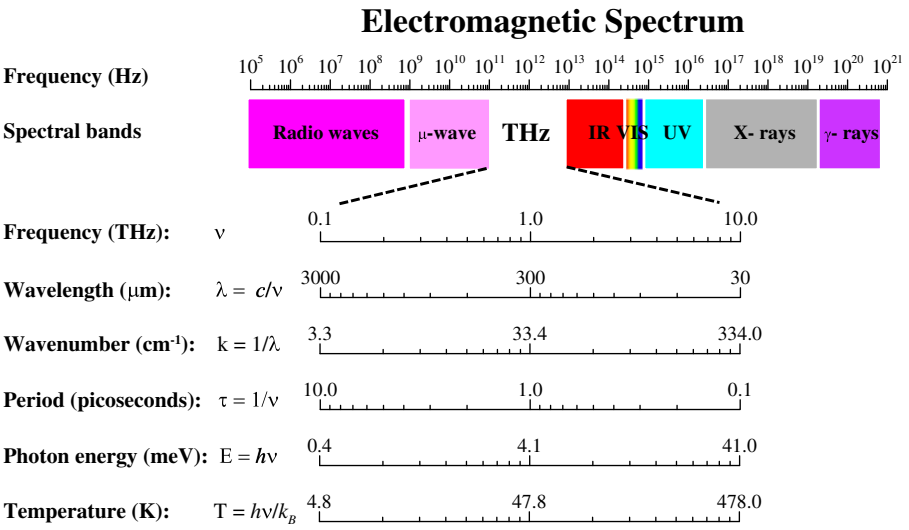

Fig. 1 The Terahertz (THz) band of the electromagnetic spectrum.

sensing techniques are presently used at major airports for security screening purposes [1, 2], at major medical centers for cancer and burn diagnosis [3–8], and at border patrol checkpoints for identification of concealed explosives, drugs, and weapons [9–11].

Widespread deployment of new THz applications has prompted increased scientific interest regarding the biological effects associated with this frequency range. In recent years, many timely investigations have been performed to investigate the possible biological effects associated with THz radiation [12–22]. Unfortunately, however, a comprehensive review has not yet appeared in the literature which both discusses the fundamental interaction mechanisms, and also critically reviews the bioeffects studies that have been conducted to date. Thus, the purpose of this review is twofold. First, to provide readers with a common reference, which contains the necessary background concepts in biophysics and THz technology that are required to both conduct and evaluate THz biological research. Second, to provide a review and analysis of the studies reported in the literature on the topic of THz bioeffects.

This review is divided into seven sections. The first section provides a general introduction to the THz spectral band. The second section describes the composition and function of biological structures: skin tissue, mammalian cells, organelles, and biological macromolecules. The third section provides an overview of the fundamental mechanisms governing the interaction of THz radiation with biological materials. It also discusses energy deposition processes and temperature transients that result from THz irradiation of materials. The fourth section summarizes the primary thermal effects that are observed in biological materials at an organism, tissue, cellular, organelle, and molecular level. The concepts described in this section are valuable because they provide the foundation to understand THz-induced effects at all levels of biological organization. In addition, they give the reader the tools to determine whether the effects observed in THz reports can be fully attributable to the temperature rise generated during exposure. The fifth section surveys the major types of THz sources, detectors, and equipment that are used in biological research. This section also addresses the common challenges and considerations

that investigators face in this field. Following the description of THz technologies, the sixth section then describes our methodology to survey the literature. This section provides a comprehensive review and "study-by-study" analysis of the THz bioeffects reports that appear in the literature. The review concludes with a summary section that addresses challenges and future opportunities in this field.

2 Background: composition and function of biological structures

THz-induced biological effects are influenced by two general factors: the THz exposure parameters (i.e., frequency, power, exposure duration, etc.) and the composition and/or properties of the biological target. This section provides background on the chemical composition and function of skin, the largest and primary biological target for THz radiation. Please note, the cornea is also an important biological target for THz radiation; however, in an effort to make this section more concise we have not provided details for this tissue. This section also serves to provide the necessary foundation that is required to understand the biological origin of tissue optical properties.

2.1 Human skin: structure and chemical composition

Skin consists of two primary layers: an outer epidermis and an underlying dermis (Fig. 2a). The epidermis consists of water, keratin proteins, melanin granules, and several cell types, including langerhans, melanocytes, and keratinocytes. The main function of the epidermis is to provide a physical barrier that not only protects against water loss, but also prevents harmful external agents from entering. This protective barrier is achieved by keratinocytes. Roughly 95% of all epithelial cells are keratinocytes, thus, they are the most common type of skin cell. Keratinocytes are genetically programmed to undergo a cellular differentiation process known as keratinization.

The keratinization process results in the formation of a layered barrier referred to as a stratified squamous tissue. Squamous epithelial tissue consists of five distinct layers or strata: stratum corneum (sc), lucidum (sl), granulosum (sg), spinosum (ss), and basale (sb) (Fig. 2a). Keratinocytes undergo several phenotypic changes as they progress from the inner to the outer stratum. In brief, these changes include: increases in keratin production, decreases in water content, decreases in cellular metabolism, loss of nuclei and organelles, and cellular flattening.

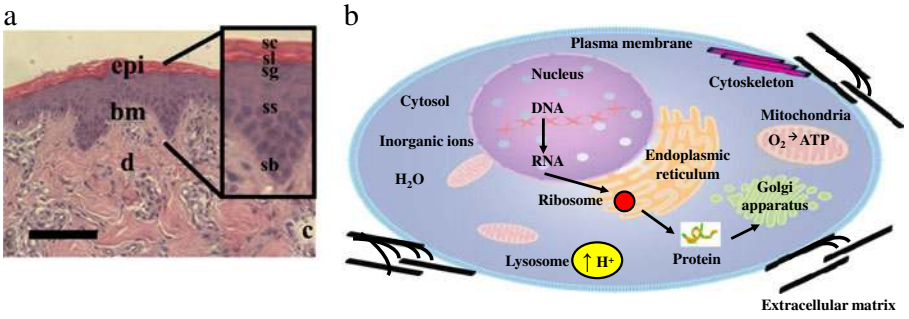

Fig. 2 (**a**–**b**). **a**. Skin anatomy. Histological cross section of porcine skin tissue (Hematoxylin and Eosin stain at 40X magnification). Epidermis (epi), basement membrane (bm), dermis (d). Legend for magnification: stratum corneum (sc), stratum lucidum (sl), stratum granulosum (sg), stratum spinosum (ss), and stratum basale (sb) **b**. Cellular chemistry and morphology. Image created with Ingenuity IPA software.

Although keratinocytes in the sb layer are devoid of keratin, they do have high concentrations of melanin, a pigment responsible for skin color (i.e., Fitzpatrick skin type). Melanin granules are produced by melanocytes, and they are transferred to keratinocytes via cytocrine secretion mechanisms. To date, studies have not been performed to characterize the optical properties of melanin at THz frequencies; however, comparable studies have been conducted at optical frequencies. These studies report that the absorption coefficient (μ_a) of melanin decreases with wavelength, and can be approximated as: μ_a (cm^{-1}) = $1.70\times10^{12}\times\lambda^{-3.48}$ (nanometers, nm) [23]. Assuming this trend continues into the THz region, melanin absorption is probably weak at THz frequencies (i.e., $\mu_a \leq 10^{-4}$ cm^{-1}).

In addition to contributing to skin color, the sb layer also assists in formation of the basement membrane (BM). The BM is the layer that separates the epidermis and dermis. It consists primarily of type IV collagen, laminin, entactin, and sulfated proteoglycans. Interestingly, to date, few studies have characterized the optical properties of these biomolecules at THz frequencies [24]. Such information would likely improve the accuracy of computational models that are currently used to predict THz-tissue interactions.

Immediately below the epidermis lies the dermis. The dermis provides skin with shape and structural integrity, and it ranges in thickness across the human body between 0.3 and 4 millimeters (Fig. 2a). The dermis consists of dermal fibroblasts that are anchored in an extracellular matrix (ECM). The ECM consists of fibrillar collagen embedded in a ground substance material. It is interesting to note that healthy fibrillar collagen exhibits a characteristic banding pattern with a periodicity of ~60 nm, whereas thermally damaged collagen loses this signature banding pattern. The significance of this feature will be described in greater detail in Section 4.1. Ground substance is primarily comprised of water, collagen, elastin, proteoglycans, and gylcosaminoglycans (GAGs). GAGs are hydrophilic molecules that sequester water volumes roughly 1000 times their own volume [25]. Due to this property, large volumes of water typically reside in the ground substance of the dermis. This property is important to note because water is the primary chromophore at THz frequencies, thus, its presence strongly governs where THz energy is deposited (see Sections 3.1-3.3).

2.2 Structure and chemical composition of mammalian cells

Cells in the human body come in a wide variety of sizes and shapes; however, virtually all cells share certain characteristics (Fig. 2b). First, all cells are enclosed by an outer protective barrier known as the plasma membrane. The plasma membrane provides a selective barrier between intracellular contents and extracellular fluids. The plasma membrane is composed of a phospholipid bilayer, which contains integral proteins and cholesterol. The phospholipid bilayer is comprised of two elements: hydrophilic polar heads, which are oriented towards the outer surface, and hydrocarbon tails which are present in the interior of bilayer in the interior. The degree of saturation of the carbon-carbon bonds in the hydrocarbon tails governs the structure and order of the bilayer, where saturated hydrocarbons chains are more restricted and unsaturated chains are more fluid [26]. Overall, the properties and thermal sensitivity of plasma membranes depend on the cell type, exact membrane composition, and ratio of saturated versus unsaturated hydrocarbons [27].

Two distinct regions exist inside the plasma membrane of all cells: cytosol and cytoplasm (Fig. 2b). The cytosol makes up the largest volume of cells, and it is primarily composed of water, organic and inorganic ions (i.e., sodium, potassium, magnesium, calcium, phosphate, and chloride), and cytoskeleton filaments. Cytoskeleton filaments provide structural support to cells, and they also play key roles in intracellular transport and cellular division. The cytoplasm is a thick alkaline (pH ~7.1–7.2) liquid that contains all

organelles [27]. Organelles are specialized membrane-bound compartments that provide vital cellular functions. The primary organelles that are present in virtually all cells are lysosomes, mitochondria, endoplasmic reticulum, and the Golgi complex (Fig. 2b).

Lysosomes are small compartments that are responsible for digesting damaged macromolecules, which are collected during autophagy, endocytosis, and phagocytosis processes. Digestion is performed within lysosomes by lipases, proteases, and other pH-sensitive hydrolase enzymes [28]. Lysosomes use membrane hydrogen proton pumps to maintain their highly acidic internal environment (pH<4.8) [26]. In addition to their waste disposal functions, lysosomes also assist in the sealing and repair of damaged plasma membranes [29] (Fig. 2b).

Mitochondria are a second class of cytoplasmic organelles that are present in nearly all cells. Nicknamed 'the powerhouse of the cell,' the main function of mitochondria is to generate chemical energy in the form of adenosine triphosphate (ATP). In the mitochondria, aerobic respiration mechanisms, such as the Kreb's cycle and oxidation phosphorylation, mediate the conversion of biochemical energy from nutrients and oxygen into the form of ATP. In addition to producing ATP, mitochondria also function as a transient storage site for calcium (Ca^{+2}), a cation required for many cellular functions, such as signal transduction, apoptosis, and cellular proliferation. Calcium entry into the mitochondrial matrix is driven by a steep electrochemical proton gradient provided by the mitochondrial membrane potential ($\Delta\Psi_m$) equal to −100 to 220 mV [30]. Interestingly, maintenance of a low $\Delta\Psi_m$ is directly linked to the formation and generation of free radicals and reactive oxygen species (ROS) [31]. Furthermore, recent data suggest that ROS production increases exponentially at $\Delta\Psi_m$'s greater than 140 mV [30]. Overall, mitochondria play critical roles in ATP production, cellular metabolism, signal transduction, and redox (Fig. 2b).

The endoplasmic reticulum (ER) and the Golgi complex are the final two major cytoplasmic organelles that are present in most cells. The primary function of the ER is to synthesize and deliver nascent proteins, lipids, and steroids to the Golgi complex. Once delivered to the golgi complex, these macromolecules are then packaged and delivered to their final destination within the cell (Fig. 2b).

The nucleus is the largest and perhaps the most important cellular organelle. The nucleus contains the majority of a cell's genetic material (i.e., DNA and RNA), and it is sometimes referred to as the cell's 'control center.' The primary functions of the nucleus are to regulate cellular gene expression, provide a site for mRNA transcription, and to facilitate DNA replication [26] (Fig. 2b).

3 Terahertz interactions with biological materials

The interaction of THz radiation with biological materials is influenced by two primary elements: (i) THz exposure parameters (i.e., frequency, spot size, exposure duration, irradiance, and beam profile); and (ii) the composition and properties of biological materials (i.e., index of refraction, absorption properties, and scattering properties). As a result, both of these elements can impact the propagation, spatial distribution of energy, and thermal effects resulting from THz irradiation of biological materials. Therefore, knowledge of the fundamental principles governing these processes is necessary to understand the biological effects associated with THz irradiation. This section provides the following: an overview of the principles governing the interaction and propagation of THz radiation in biological materials (Section 3.1): an examination of the biological origins of absorption and scattering phenomenon (Section 3.2); and a discussion on energy deposition, temperature transients, and thermal responses of biological materials (Section 3.3).

3.1 Fundamental principles of THz-material interactions

When THz photons interact with a material, a fraction of the photons are reflected at the material boundary, and the remaining photons are transmitted into the material. Figure 3a is a graphical representation of an incident THz wave being reflected and transmitted into skin. Assuming a unit incident irradiance Φ_o (Wm^{-2}), the light transmitted into the tissue can be defined as: $T = 1 - R_s$, where T and R_s represent the ratio of transmitted and specular reflected photons, respectively.

Two factors directly contribute to the amount of specular reflectance loses at a material interface: (i) the angle of incidence θ_1 of the incoming THz beam; and (ii) the index of refraction n mismatch between air (n_1) and the sample material (n_2). The relationship between these entities can be computed using Snell's Law, $n_1 \sin \theta_1 = n_2 \sin \theta_2$, where θ_1 is the angle of incidence in air ($n_1 \approx 1$), and θ_2 is the angle of refraction in the material (n_2).

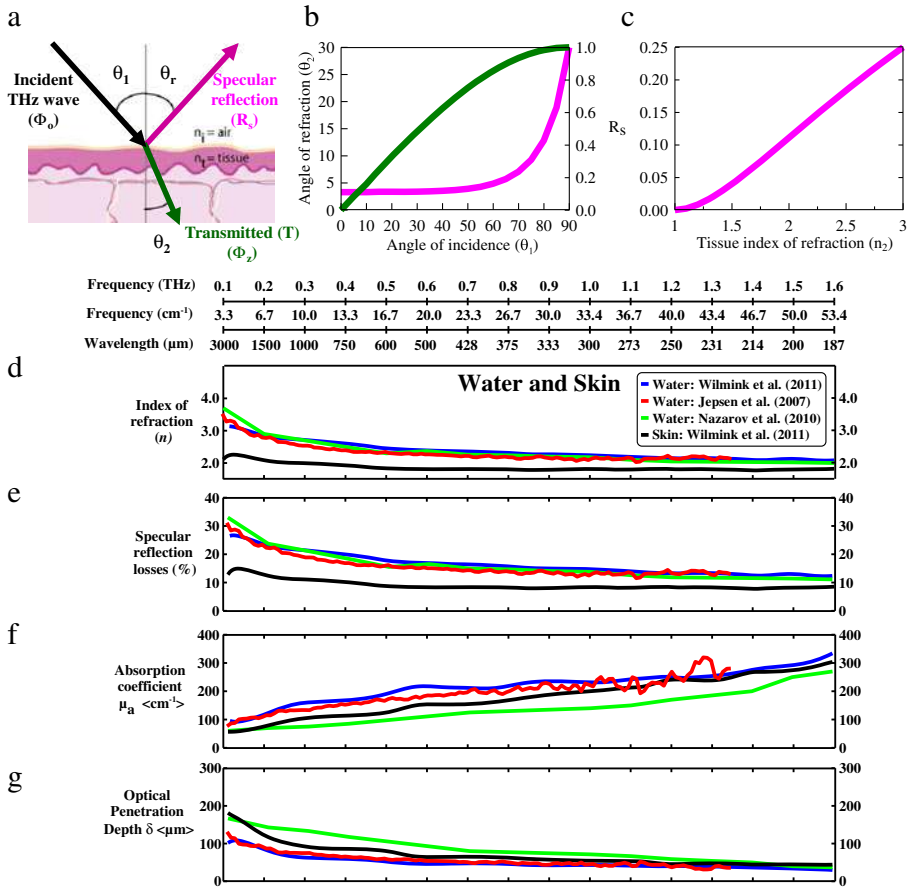

Fig. 3 (a–g) THz interactions with biological materials. **a**. Image illustrating THz beam attenuation in biological materials. **b–c**. Graphical representations illustrating the relationship between angle of incidence, angle of refraction, tissue index of refraction, and magnitude of specular reflection. **d–g**. Real index of refraction (n), specular reflection loses (R_s), absorption coefficient (μ_a). and optical penetration depth (δ). Water spectra: Wilmink *et al.* [182], blue line; Jepsen *et al.* [41], red line; Nazarov *et al.* [183]; green line. Skin spectra: Wilmink *et al.* [182], black line.

Neglecting polarization, the magnitude of specular reflectance can be approximated using the Fresnel relation:

$$R_s = \frac{1}{2}\left(\frac{\tan^2(\theta_1 - \theta_2)}{\tan^2(\theta_1 + \theta_2)} + \frac{\sin^2(\theta_1 - \theta_2)}{\sin^2(\theta_1 + \theta_2)}\right), \quad (1)$$

Figure 3b is plot of θ_1 versus the magnitude of R_s. The data illustrate that the magnitude of R_s increases exponentially for angles of incidence greater than 60 degrees. Assuming the angle of incidence is normal to the material, Eq. 1 reduces to:

$$R_s = \left(\frac{n_1 - n_2}{n_1 + n_2}\right)^2, \quad (2)$$

Figure 3c is a graphical representation that illustrates the relationship between a material's index of refraction and the magnitude of Rs. The data clearly show that increases in a material's index of refraction result in appreciable increases in R_s. Figure 3d contains published data for the index of refraction of water and porcine skin at THz frequencies [32–43]. The data shows that water's index ranges from 3.5 at 0.1 THz to 2.0 at 1.6 THz, while skin's index ranges from 2.2 at 0.1 THz to 2.0 at 1.6 THz. Corresponding R_s values are provided in Fig. 3e. The data show that only 70 to 90% of the incidence THz irradiance is transmitted into biologic materials. Clearly, the air–tissue interface leads to substantial losses.

After accounting for R_s, the transmission T of THz photons can then be determined using Beer-Lambert's law:

$$T = \frac{\Phi_z}{\Phi_o} = e^{(-\mu_a z)}, \quad (3)$$

where Φ_o is the incidence irradiance (Wm^{-2}), Φ_z is the irradiance (Wm^{-2}) after traveling through a path length z in the material, and μ_a is the absorption coefficient of the material. The absorption coefficient μ_a (cm^{-1}) is defined as the probability that a photon is absorbed per infinitesimal unit path length. The reciprocal of μ_a is referred to as the mean absorption length or the optical penetration depth δ (m). This value corresponds to the depth where the irradiance is equal to 1/e, or roughly 37% of the incidence irradiance.

In addition to absorption, the scattering properties of materials can also impact the spatial distribution of deposited photons. Analogous to the absorption coefficient, the scattering coefficient μ_s (cm^{-1}) is defined as the probability of photon scattering per infinitesimal unit path length. Scattering arises from spatial variations in the refractive index of the tissue, extracellular constituents, and mammalian cells. Photons scatter most strongly by structures whose size matches the incident wavelength. Thus, scattering in biological materials is strong at visible and near-IR wavelengths, and weak at longer wavelengths. Biological scattering is particularly weak at THz wavelengths because THz waves are several orders of magnitude larger than most biological structures. Due to this feature, THz-tissue interactions are assumed to be an absorption-dominated case.

3.2 Biological origin and absorption properties of skin at THz frequencies

Many biological macromolecules (i.e., DNA, proteins, tryptophan, and carbohydrates) contribute to tissue absorption, but most data suggest that water is the chief tissue chromophore at THz frequencies [44–48]. Water exhibits many unique properties that contribute to its strong interaction with THz radiation. One such property is the ability of

water molecules to readily engage in both inter- and intra-molecular hydrogen bonding with neighboring molecules. As a result of these interactions, water molecules create extensive dynamic hydrogen bond networks that behave in a collective manner. Interestingly, the intermolecular stretching vibrations of this network, which are the origin of macroscopic water dynamics, are quite strong at a frequency of 5.6 THz [49–51]. In addition, due to the slow relaxation time of bulk water molecules, large intermolecular bending vibrations occur at 1.5 THz [49–51]. In addition to water, many other biological macromolecules also exhibit collective vibrational modes at THz frequencies [52–56]. Overall, many biological macromolecules contribute to the tissue absorption, but water is believed to be the main chromophore at THz frequencies.

The optical properties of skin and water, the primary constituent of all biological tissues, are well-characterized at THz frequencies. Figure 3(f-g) contains the absorption values and corresponding optical penetration depths (δ) for water and *ex vivo* porcine skin. The absorption coefficient of water and skin are comparable and range in value between 100 cm^{-1} at 0.1 THz to 300 cm^{-1} at 1.6 THz [42, 57]. The data also shows that the optical penetration depth is a few hundred microns at lower THz frequencies, and roughly fifty microns at higher THz frequencies.

3.3 Thermal response of tissue

When THz energy is transmitted into biological materials, the optical energy is absorbed by target chromophores. Once absorbed, this energy is then converted into heat, and in the process generates significant thermal transients, which are the driving force and precursor for all photothermal processes. Thus, in the absence of photochemical processes and phase transitions, all energy absorbed by THz-exposed tissue is converted into a temperature rise. Using the incident THz irradiance and the absorption coefficient for skin, the rate and amount of energy that is deposited into the tissue can be calculated. This rate is typically defined as the rate of heat generation S (Wm^{-3}):

$$S(r,z) = \mu_a(r,z)\Phi_o(r,z), \tag{4}$$

where Φ_o (r,z) is the irradiance at a point located in the tissue at (r,z), and μ_a is the local absorption coefficient at point (r,z). Then using S computed in Eq. 4, the local temperature rise in the tissue can be calculated using the following relationship:

$$\Delta T(r,z) = \frac{S(r,z)\Delta t}{\rho c}, \tag{5}$$

where ΔT is the local temperature rise in (Kelvin) at an arbitrary location r, Δt is the duration of the heat exposure, ρ is the tissue density (gm^{-3}), and c is the tissue's specific heat capacity in ($Jg^{-1}K^{-1}$).

Once the energy absorption terms are determined, the Pennes' bioheat equation, which is based on the heat diffusion equation, can be used to model heat transfer [58, 59]:

$$\rho c\frac{\partial T}{\partial t} = k\nabla^2 T + S + \overline{q} \tag{6}$$

where ρ is the density of the water or tissue (kg m^{-3}), c is the specific heat (J $kg^{-1}K^{-1}$), T is the temperature (Kelvin), t is the exposure duration (seconds), κ is the thermal conductivity

($Wm^{-1}K^{-1}$), S is the heat of generation , and q is the rate of perfusion. Equation 6 can then be converted into 3−D Cartesian domains:

$$\rho c \frac{\partial T}{\partial t} = \frac{\partial}{\partial x}\left(k\frac{\partial T}{\partial x}\right) + \frac{\partial}{\partial y}\left(k\frac{\partial T}{\partial y}\right) + \frac{\partial}{\partial z}\left(k\frac{\partial T}{\partial z}\right) + s + \overline{q} \tag{7}$$

These equations can then be used with computational modeling and simulation (M&S) techniques, such as Monte Carlo and Finite-difference-time-domain (FDTD) methods, to model the propagation and deposition of THz photons in biological tissues. For further details on M&S we refer the reader to several books [58, 60].

4 Thermal effects in biological materials

Biological materials exposed to THz energy can undergo changes at various levels. Common effects include tissue coagulation, structural protein damage, cell death, activation of intracellular stress responses, and disruption of cellular organelle functions. Furthermore, since THz energy is strongly absorbed by biological tissues, higher levels of THz power are likely to generate pronounced thermal effects in biological materials. Thus, knowledge of conventional thermal effects and their respective time-temperature histories is essential for proper analysis of THz bioeffects studies.

In this section, we shall provide a summary of the principle thermal effects observed in biological structures. Clearly, this field is too broad for a section of modest length, so we have chosen to only highlight the signature signs of hyperthermic damage. Here we describe the thermal effects of organisms, tissues, extracellular proteins, mammalian cells, cellular organelles, and biological macromolecules. This section is organized with the intention of providing the reader with a framework to understand the pleotropic effects of hyperthermia.

4.1 Thermal effects on organisms and biological tissues

The type and severity of thermal effects depends on many factors: (i) exponentially dependent on temperature; (ii) linearly dependent on the duration of exposure; (iii) organism, tissue, and cell type; (iv) tissue architecture and macroscopic environment (i.e., blood perfusion, hydration levels); and (v) metabolism, physiology, and microenvironment of cellular constituents (i.e. pH, O_2, CO_2, ATP, glucose, and metabolite levels)[27]. These factors vary widely in different biological materials, thus, each material exhibits vastly different thermal sensitivities. Clearly, given the large number of variables that contribute to thermosensitivity, it is difficult to determine the exact thermosensitivity of a particular biological material. However, all biological materials exhibit similar response trends that can be used to relate dosimetry with observed effects.

Hyperthermia causes several effects at the organism and tissue level. The most common effects include: (i) activation of acute inflammatory responses; (ii) tissue dessication and necrosis; and (iii) irreversible structural protein denaturation, birefringence loss, and visible tissue whitening [61–63] [Fig. 4(a-b)]. The sensory nerves that reside in skin perceive hyperthermia to be a harmful stimulus, and consequently respond to it by activating an acute inflammatory response. This response, which typically lasts several days, functions to not only remove injurious stimuli, but also to initiate the wound healing cascade. The

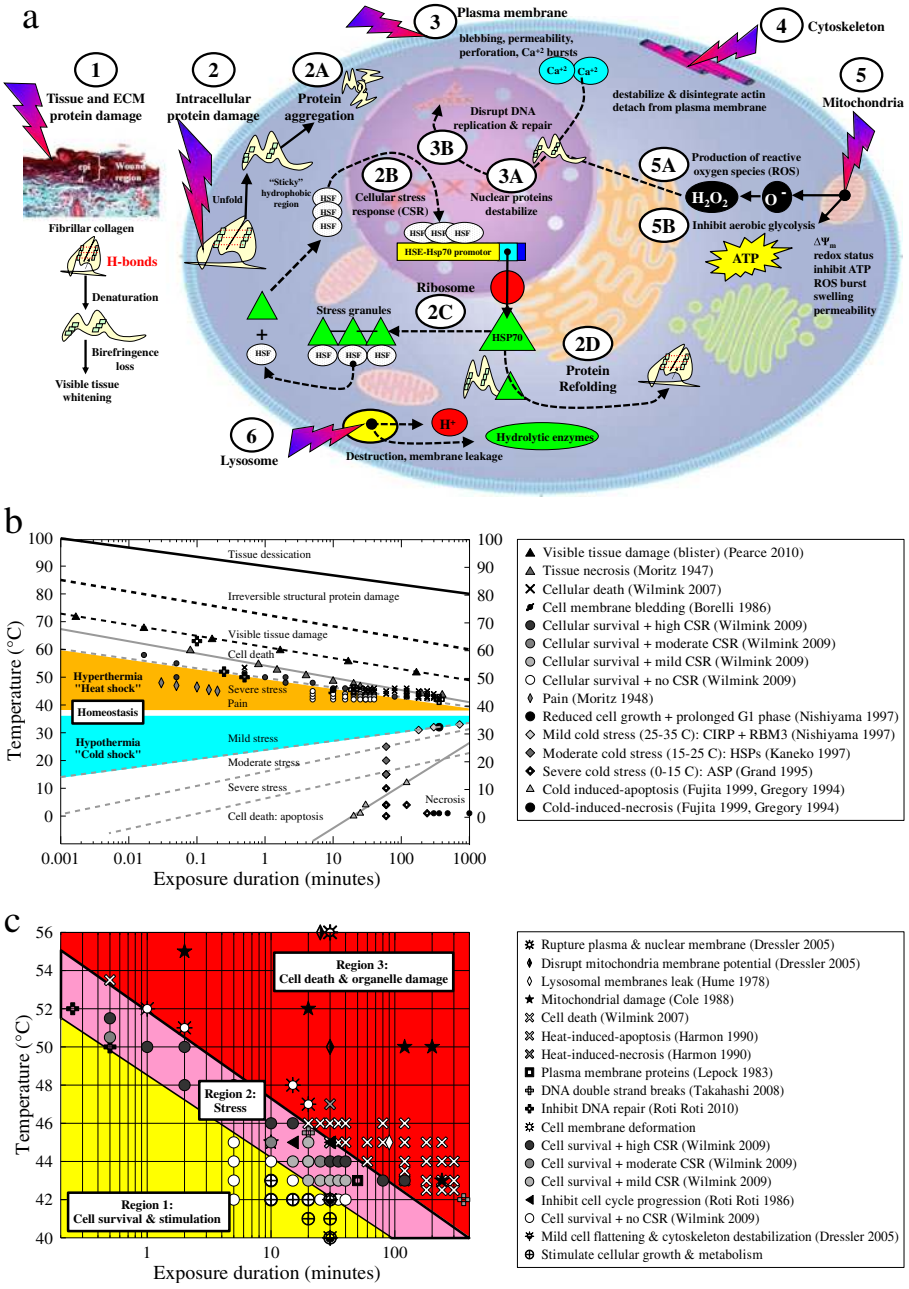

Fig. 4 (**A**–**C**) Thermal effects of tissues, cells, organelles, and biological macromolecules. **a**. A cartoon graphic illustrating the effects of THz radiation on tissue and extracellular collagen proteins (1), intracellular proteins (2), plasma membranes (3), actin cytoskeleton (4), mitochondria (5), and lysosomes (6). **b**. Thermal effects of tissues with exposure temperature plotted versus exposure duration. **c**. Thermal effects of cells, organelles, and macromolecules.

cardinal signs of inflammation are: pain, heat, redness, and swelling. These signs are primarily the result of the increased blood flow that is used to facilitate the movement of white blood cells into the injured tissue region.

Biological tissues typically become desiccated and necrotic when exposed to elevated temperatures ranging between 80–100°C for several seconds. In contrast, irreversible damage extracellular proteins can occur at considerably lower temperatures ranging between 50–70°C for several minutes [61] [Fig. 4(b)]. In fact, structural proteins, such as fibrillar collagen, are often damaged when tissue temperatures reach 60°C for 1 minute or longer [64]. When structural proteins are irreversibly damaged they become visibly whiter. Tissue whiting is a consequent of the biřefringence loss that occurs when the regular arrangement of collagen molecules is disrupted (see Section 2.1).

Figure 4a contains a cartoon graphic illustrating the effect of hyperthermia on tissue and extracellular collagen proteins (Pathway 1, far left). The image provided in the figure is a histological cross section of heated skin stained with a Gomori Trichrome collagen stain. The image illustrates that the denatured collagen in the wounded skin region stains red, whereas the healthy collagen in the untreated skin region stains green. Often times, tissue effects are more subtle, and are not clearly visible. For these instances, tissue damage assessment requires microscopic techniques, such as transmission polarizing, transmission electron, and multi-photon microscopy. It is important to note that visible tissue damage is used as a biological endpoint for the determination of safety standards at optical and higher THz frequencies (i.e. ANSI standards). Thus, knowledge of the thermal effects of tissue is important for the determination of safety standards at THz frequencies [65]. A summary plot of hyperthermic tissue effects is provided in Fig. 4b.

4.2 Thermal effects on mammalian cells

The most common thermal effects observed at a cellular level include the following: (i) stimulation of cell growth and metabolism; (ii) morphological changes (i.e., swelling, blebbing, shrinking); (iii) activation of cellular stress response (CSR) mechanisms [66–69], and (iv) cell death via apoptotic and necrotic pathways [66–69]. The thermal sensitivity of cells is cell type dependent; however, all cell lines typically share a similar response trend. This trend can be generalized and grouped into three distinct time-temperature dosimetry regions, where region 1, region 2, and region 3 comprise the effects observed for increasing levels of hyperthermia (Fig. 4a, c).

Temperatures ranging between 40–42°C are typically not lethal to most cells (Fig. 4c, Region 1). However, such exposures can lead to subtle morphological alterations, such as cell flattening and membrane ruffling. These effects are believed to be a result of cytoskeleton reorganization and mild destabilization of actin-plasma membrane connections [70]. Consistent with this theory, Dressler *et al.* demonstrated that cells exposed to mild heat stress (40 and 42°C for 30 min) maintained their structural integrity, but their F-actin network appeared mildly destabilized, giving the cells a flattened appearance [70]. Clearly, mild hyperthermia can lead to subtle morphological effects; however, such exposures also activate intracellular signaling pathways, such as cellular growth and metabolic processes [66, 69, 71] (Fig. 4c). In fact, mild thermal stress (40–42°C for 10–30 min) has been shown to increase the growth and metabolic rates of cells by 20% [66, 69, 71, 72].

Mammalian cells exposed to temperatures ranging between 42–46°C for 30–50 min (Fig. 4c, Region 2) typically exhibit several signature effects: (i) dramatically altered cellular morphology (i.e., shape, size, irregularities, and roughness); (ii) reduced adhesion to ECM and intracellular actin cytoskeleton; (iii) inhibition of cell cycle progression; and (iv) activation of a molecular

defense reaction called the cellular stress response (CSR). Specifically, Dressler *et al.* demonstrated that cells exposed to 45°C for 30 min exhibit a disintegrated actin network, a rough and irregular plasma membrane, a decrease in cell size, and spheroidal cell shape [70].

In addition to these structural and morphological effects, temperatures ranging between 43–44°C for 15–50 min can also result in the impairment of cell cycle progression and/or cause the triggering of CSR mechanisms. For example, cells exposed to 45°C for 15 min were observed to undergo transient G_2 block, while when exposed to 45°C for 30 min, they exhibited a long lasting G_2 phase and a late S-phase block [73]. The CSR mechanism is well documented in the literature [66–69, 74–77], and the general consensus is that cells activate these mechanisms to combat and survive hyperthermic stress. CSR mechanisms involve many intracellular pathways, including redox, DNA sensing and repair, molecular chaperones, proteolysis, energy metabolism, and apoptosis [78]. Many proteins are associated with these pathways; however, a group of 44 evolutionary conserved proteins have emerged as core mediators [79]. These proteins, collectively referred to as minimal stress proteins, are significantly upregulated by cells immediately after exposure to stress. The most widely studied family of minimal stress proteins are the heat shock proteins (Hsps), which includes Hsp70, Hsp40, Hsp60, and Hsp105 [66–69, 74–77] (Fig. 4a, c).

Mammalian cells exposed severe thermal stress with temperatures greater than 46°C (i.e., ablative regime) exhibit gross alterations to most cellular components (Fig. 4c, Region 3). These effects include the collapse of cellular shape, complete destabilization and disintegration of actin cytoskeleton network, rupture of both plasma and nuclear membranes [70], and cell death via apoptotic and necrotic pathways (Fig. 4a, c). In general, cells preferentially activate apoptotic pathways when they have the resources available (ATP, oxygen, *etc*); however, when resources are unavailable, cells die via necrosis pathways [80].

Finally, in addition to hyperthermia, hypothermia or cold shock temperatures can also cause severe cellular effects (Fig. 4b). Cold shock effects are typically divided into three time-temperature categories: (i) Mild (25–35°C); (ii) Moderate (15–25°C); and (iii) Severe (0–15°C). Under mild cold shock conditions cells express cold-inducible proteins (CIRP), while at more moderate conditions they express both HSPs and apoptosis-specific proteins (ASPs) [81–83]. At this point it may not be clear to reader why we have decided to address the effects of hypothermia. The relevance and importance of hypothermia- based effects will become clearer in subsequent sections. In brief, many THz bioeffects studies expose cells under cold shock conditions, thus, knowledge of hypothermia-induced cellular effects is critical to differentiate the origin of such effects.

4.3 Thermal effects on cellular organelles

Hyperthermia can cause direct effects to cellular organelles. Damage to organelles is often times a direct consequent of damage to the outer membranes of each major organelle. In this section, we shall briefly describe the thermal effects that are frequently observed on the plasma membrane, cytoskeleton, mitochondria, lysosomes, and nucleus.

Heat can cause several changes to the plasma membrane and its interconnected actin cytoskeleton. These effects include gross morphological changes, redistribution of membrane proteins, actin-plasma membrane detachment, membrane perforation, changes in membrane permeability, and spikes in intracellular calcium levels [70, 84–86] (Fig. 4a, c). Although surprising, given the fact that the plasma membrane provides vital cellular protection, several groups have provided compelling evidence that the plasma membrane may be the most thermosensitive cellular component [70, 87]. In fact, a recent study showed that morphology changes were observed in cells heated at 45°C for 30 min. These effects are believed to be a

direct result of cytoskeleton detachment from the plasma membrane. Data from this study also showed that these effects are continuously enhanced over the 40 to 56°C temperature range [70].

The thermal sensitivity of plasma membranes depends on the composition and properties of the local membrane. These properties depend on the levels of cholesterol, membrane proteins, and the ratio of saturated to unsaturated fats. Thus, since membrane composition varies with cell type, the thermal sensitivity of cells also depends on cell type. The effect that membrane composition has on thermosensitivity has been highlighted in several studies [88, 89]. These studies specifically showed that cells supplemented with polyunsaturated fatty acids had increased thermosensivity, whereas cells supplemented with saturated fatty acids had decreased thermosensivity [88, 89].

Heat can cause several interrelated effects on mitochondria: (i) disrupt membrane potential ($\Delta\Psi_m$)[84, 90]; (ii) change the redox status of cells; (iii) cause increased bursts of ROS; (iv) stimulate mitochondrial enzyme activity (i.e. citrate synthase)[87]; (v) inhibit ATP production; and (vi) destabilize intracellular proteins (Fig. 4a, c) [27]. Membrane disruption typically does not occur under mild heat stress (40 and 45°C for 30 min), but it becomes quite pronounced under severe conditions (50–56°C for 30 min) [90]. Membrane disruptions are believed to be mediated via the signaling of pro-apoptotic (Bax) and anti-apopotic Bcl-2 family members, in particular caspase 2 [91]. In combination, these effects are believed to directly affect cellular redox, increase the generation of ROS, reduce citrate synthase activity by almost 50%, and ultimately reduce the production level of ATP [87, 91]. In fact, a recent study showed that cells decrease their ATP content by nearly 60% when exposed to a 20 min heat shock at 45°C [87]. These primary effects can also lead to the destabilization of both cytosolic and nuclear proteins, which can lead to activation of CSR mechanisms, and DNA damage.

Heat can cause several effects on lysosomal membranes [92–95]. Heat stress at temperatures ranging between 41 and 43°C for 90 min durations can trigger increases in lysosomal enzyme activity [95]. In addition, higher temperatures, such as 45°C for 90 min, can make lysosomal membranes leaky, resulting in the release of hydrogen and hydrolytic enzymes into the cytosol. Thus, these primary effects can cause drastic secondary effects, such as proteolysis deficiencies and impaired cellular function.

The nuclear membrane has long been considered the most thermoresilinient cellular organelle. This theory seemed reasonable given the fact that temperatures of 56°C for 30 min are required to puncture the nuclear membrane [70]. A more recent report, however, provided definitive evidence that the nucleolus is a repository of stress responsive proteins that are released in response to thermal stress [96]. This work also provided evidence that a critical underlying nuclear structure, referred to as the nuclear matrix, is the most temperature sensitive subcellular component identified to date [96]. The nuclear matrix plays several vital functions, including DNA replication, RNA processing, and DNA repair. Thus, heat shock has the potential to disrupt many critical functions of the cell, and thus may be the key mechanism underlying cell death. For further details on the thermal effects of the nucleus, we refer the reader to the following articles [73, 84, 97, 98].

4.4 Thermal effects on biological macromolecules

The thermal effects observed at a cellular and organelle level are a direct result of damage to intracellular biomolecules. At a molecular level, when biological tissues are heated, the ensuing temperature rises increase the kinetic energy of the tissue's water and biomolecules. When this

excitation energy exceeds the energy provided by the intramolecular bonds, which holds the molecules together, biological molecules (i.e., lipids, proteins, mRNA, DNA) undergo conformational changes and/or denature. Thermal effects to macromolecules are typically subdivided into two groups, where higher thermal ablation temperatures (50–60°C) cause irreversible damage, and hyperthermic temperatures (40–48°C) cause reversible damage. Common reversible effects include the deactivation of enzymes, protein unfolding or denaturation, and acceleration of cellular metabolism. These effects are a direct result of the disruption of the hydrogen and disulfide bonds that maintain the tertiary structure of proteins and DNA. When intracellular proteins are reversibly damaged, mammalian cells typically activate CSR mechanisms (described above) to repair the damage (Fig. 4a). In contrast, when proteins are irreversibly damaged, cells activate proteolysis mechanisms to degrade proteins in lysosomes. For more details on the thermal effects on macromolecules we refer the reader to Urano *et al.* [27]

4.5 Microthermal biological effects

Hydrated biological tissues are known to strongly absorb radiation at THz frequencies. Thus, high-power THz radiation is assumed to cause thermal effects in biological materials. In addition to conventional thermal effects, however, several researchers have proposed that THz radiation may also induce low-level thermal, nonthermal, or more appropriately, microthermal effects. These theories were initially hypothesized by Frohlich *et al.* in 1971 [99, 100], and more recent studies propose that these microthermal effects are mediated through the direct coherent excitation of biomolecules [99] or linear/nonlinear resonance mechanisms [101, 102].

In recent years, several research groups have conducted extensive efforts to develop more established theoretical frameworks to support the concept of "nonthermal" effects [101, 103, 104]. These studies suggest that nonthermal coupling mechanisms may be due to the fact that THz radiation (i.e., THz = 10^{12} Hz) oscillates on the same time scale (picoseconds) as the natural phonon frequencies of biological molecules [101, 102]. Interestingly, these models also contend that the coupling of THz radiation to DNA may create localized openings "bubbles" between the DNA strands. Such openings are believed to drive double-stranded DNA (dsDNA) to "unzip" and interfere with transcription processes [101, 102].

Modern tools are not available to detect microthermal effects; therefore, it is difficult, if not impossible, to verify the existence of such effects experimentally. As a result, the concept of these effects has remained a constant subject of debate [105, 106]. However, since many observed effects reported in the THz bioeffects literature cannot be readily explained by the temperature rise generated during irradiation (i.e., conventional thermal effects) we believe that it is important that the reader is aware of these potential mechanisms and effects.

5 Terahertz biological research

Although an extensive review on THz sources, detectors, and technologies is beyond the scope of this review, a brief overview of equipment commonly used in THz biological research is valuable for subsequent bioeffects discussions. For additional details about THz technologies we refer the reader to several excellent reviews and books [107–116]. In this section, we provide an overview of the main sources, detectors, and equipment used in THz biological research. We then proceed by describing the systems and tools used to control

exposure conditions and conduct dosimetry. We conclude with a section describing the common challenges faced in THz biological research.

5.1 Terahertz sources

THz sources are typically categorized according to their principle operational scheme. The most common schemes used in THz biological research are the following: (i) direct generation laser sources; (ii) solid-state electronic devices (frequency up-conversion); (iii) accelerating electrons-based sources.

5.1.1 Direct generation laser sources

The three most common direct generation THz laser sources are far-infrared (FIR), electrically-pumped solid state, and quantum cascade lasers. Of these, the FIR laser is the most commonly used source for THz biological research. With initial uses dating back to the early 1960's, the FIR laser is one of the oldest THz sources [117, 118]. FIR lasers typically consist of the following components (i) pump source: a tunable high power carbon diode (CO_2) laser; (ii) laser cavity with a vacuum envelope container to house molecular gases; (iii) gain medium: low pressure molecular gases, such as methanol (CH_3OH) and (iv) intracavity waveguides to propagate THz radiation in transverse direction. In brief, lasing action is achieved using the pump laser to excite the vibrational levels of gas molecules, which have transition frequencies in the THz spectrum.

FIR lasers exhibit several characteristics that make them an ideal source for THz bioeffects studies. First, they provide high levels of average output power, with values on the order of 100 mW at many frequency lines. Notably, these power values are the highest levels of all commercially available bench-top THz sources [43, 119–122] (Fig. 5a). Second, FIRs are widely tunable to hundreds of discrete frequency lines across the THz spectral band. Fortunately for FIR users, tuning or "hopping" to each discrete frequency line is straightforward and is achieved by simply adjusting the pump laser wavelength, gas type and pressure. Third, FIRs generate THz radiation that is high quality, coherent, monochromatic, continuous wave (CW), and narrow linewidth (typically ~50 kHz). Finally, and perhaps most importantly, FIR sources are easy to operate and maintain. The main drawbacks of FIR lasers are their large footprint, weight, and expense. Systems can cost in excess of several hundred thousand dollars. In summary, FIR laser sources provide high output power, a wide range of operational frequencies, and high laser beam quality; therefore, they are a very attractive source for THz biological research. Such sources are particularly useful to researchers who are interested in investigating the frequency dependence of THz-induced biological effects.

5.1.2 Electronic THz sources using frequency up-conversion schemes

In recent years, numerous electronic devices have been developed to generate modest power levels of THz radiation at frequencies less than 1 THz. Electronic devices typically consist of a microwave synthesizer or oscillator, and a frequency multiplier element, which consists of an array of schottky barrier diodes (SBDs). In brief, the oscillator functions to generate "seed" microwave radiation, and the SBD array functions to multiply the frequency of the incoming microwave radiation to THz frequencies (i.e., frequency up-conversion)[123].

Electronic sources exhibit several design and performance features that make them useful devices for THz biological research studies. First, they are capable of providing high levels of

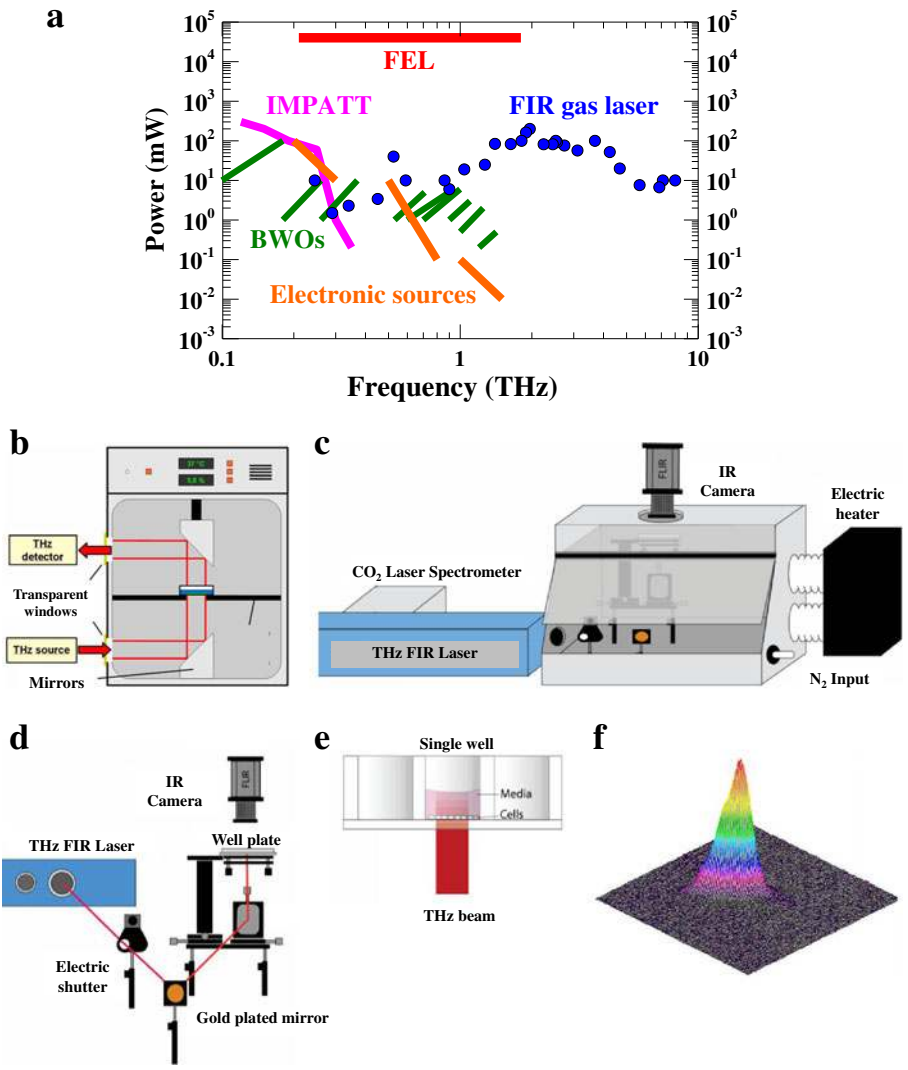

Fig. 5 (**a**–**f**) THz biological research: Sources and Equipment. **a**. Frequency-power spectrum for several THz sources. **b**. Image of a exposure chamber created using a cell culture incubator (Reprinted with permission from [145]). **c**. Macroscopic image of *in vitro* THz exposure setup: FIR THz laser source, CO_2 laser spectrometer, temperature-controlled exposure chamber, and electric heater. (Modified and reprinted with permission from [120]). **d**. Magnification of THz transmission and delivery optics: electric shutter, flat gold plated mirror, parabolic silver plated mirror, well plate holder (adjustable in XYZ), and IR camera. **e**. Magnification of THz-culture plate interaction. **f**. Sample representative image of THz beam profile at air-well interface measured with Pyrocam III detector array.

average output power (approximately 100 mW) at lower THz frequencies. Second, they generate narrow line-width (10^{-6}), CW THz radiation. Finally, they are rugged, compact, and operate at room temperature. Due to the above properties, solid state electronic THz sources are frequently used in both basic and applied research. However, despite their incredible efficiency at lower THz frequencies, such approaches are limited because they are only capable of

generating a milliwatt of power at higher frequencies [111]. In fact, recent data indicates that the output power of electronic sources drops off between $1/f^2$ and $1/f^3$ with increases in frequency [111].

In recent years, several groups have addressed the above challenges, resulting in the generation of higher power Gunn diodes [124, 125], frequency multiplier units based on SBDs, impact ionization avalanche transit-time devices (IMPATTs) [126, 127], tunneling transit time diodes (TUNNETT) [128–130], and resonant tunneling diodes (RTDs) [131]. For example, InP Gunn diodes can now generate greater than 100 mW of power at 0.1 THz and 0.1 mW at 0.48 THz [124, 125] (Fig. 5a). Several groups are also developing more advanced frequency-multiplier systems, such as varactors and varistors. Overall, electronic solid-state devices are a reliable source of low frequency THz radiation, and they are frequently used in THz bioeffects studies. With future advances in fabrication techniques, such sources may generate higher levels of output power at higher THz frequencies, and may increased use in THz biological research.

5.1.3 Accelerating electron-based THz sources

Accelerating electron-based THz sources, such as backward wave oscillators (BWOs) and free electron lasers (FELs), are frequently used for THz bioeffects investigations. Interestingly, despite their striking differences both in appearance and size, BWOs and FELs both function using the same general operation principle. Basically, both sources use a system of magnets and an external structure to generate, control, accelerate, collimate, and modulate an electron beam. The primary difference between these systems is that the external structure in a BWO is a comb grating, while in a FEL it is a wiggler system. In both systems, the external structure functions to create a periodic acceleration of the electrons in the beam, which in turn results in the generation of THz radiation. In the subsequent section, we shall explain several important features of BWOs and FELs.

BWOs are table-top devices that use electron-vacuum tubes to generate THz radiation. These devices are referred to as BWOs because they use an electron beam that travels in the *opposite* direction of a travelling EM wave. For years after their first demonstration in 1951 [133–135], BWOs were primarily developed and used in Russia. However, in recent years, several companies have increased their efforts to commercialize BWOs for use in the US and Europe.

Conventional BWOs consist of a magnetic housing system (~1 Tesla), high voltage power supply (typically, 2–6.5 kV), comb grating, cooling system, waveguide, and electron gun (cathode and anode). The frequency of the wave generated by a BWO is controlled by the velocity of the electron beam. Therefore, the output THz frequency can be directly adjusted by altering the bias voltage. Conventional BWO sources are tunable over a wide range of frequencies (0.035–1.42 THz), provide modest power levels (0.2–100 mW), and offer narrow linewidths (1–10 MHz).

BWOs were utilized in several of the initial THz bioeffects studies [136]. However, these devices have several performance and commercialization drawbacks, which have greatly limited their use. First, BWOs are quite expensive because they require sophisticated engineering and development approaches. Second, they have limited portability due to their cumbersome magnetic housing system (i.e., 27 L, 100 lbs, 1 Tesla). Finally, they have short working lifetimes (approximately 500 h). This is primarily because electron vacuum tubes wear down quickly due to their consistent exposure to extreme temperatures (1200°C), voltages (6.5 kV), and pressures (10^{-8} Torr).

Over the past few decades, several FELs have been developed to create high power THz radiation. Four THz FELs are located in the United States (Jefferson Laboratory, University

of California Santa Barbara (UCSB), University of Hawaii, and Stanford University), and several are located in Japan, Korea, Netherlands, Germany, Australia, France, Russia, and Italy. THz FELs consist of two primary components: a large electron accelerator (linac or electrostatic) and a wiggler magnetic array. The electron accelerator serves to provide a relativistic electron beam, while the magnetic field of the wiggler functions to undulate the electron beam. Electron beam modulation in turn causes the oscillation of electrons, and the emission of bright THz radiation.

THz FELs are outstanding sources for bioeffects studies because they are widely tunable both in terms of frequency and in mode of operation (CW versus pulsed). For example, the THz source at Jefferson Laboratory emits very high levels of average power on the order or 40 W, high pulse energy of roughly 3 nJ/pulse, narrow pulsewidth (350 fs), and a 75 MHz repetition rate (Fig. 5a) [137]. The primary disadvantages of FELs are the following: large footprint, require teams of researchers to run, and expensive to engineer, maintain, and operate. Despite these limitations, FELs provide the highest output power of any currently available THz source, and thus are frequently used for THz bioeffects studies [16, 17, 138–142].

5.2 Terahertz detectors

THz detectors are generally subdivided into two groups: coherent (heterodyne) and incoherent (direct) detectors. The fundamental difference between these two groups is that coherent detectors measure both the phase and amplitude of the field, whereas incoherent detectors measure only the amplitude (i.e., intensity or power) of the radiation. In general, coherent detectors are preferable in spectroscopy applications because they have a narrow spectral range and offer ultrahigh spectral resolution ($\upsilon/\Delta\upsilon \sim 10^6$). In contrast, incoherent detectors are preferable in biological research and imaging applications because they offer high sensitivity, operate over a wider spectral range, and achieve moderate spectral resolution ($\upsilon/\Delta\upsilon \sim 10^4$). These features are particularly valuable because they permit accurate power measurements at most THz frequencies, and such measurements are critical for accurate metrology, THz beam diagnostics, and dosimetric analyses.

The most common incoherent THz detectors are thermal sensors. Examples include calorimeters, bolometers, microbolometers, Golay cells, and pyroelectric devices. All thermal sensors are similar in that they each contain an absorbing element which is attached to a heat sink. The primary difference between each detector type is the means by which they measure the temperature increases. For further details on the principles of operation of thermal detectors we refer the reader to one of the following articles [111, 143, 144].

All thermal sensors share several common strengths and weaknesses. Common strengths include high sensitivity and wide spectral range operation. One common weakness is that measurements with thermal detectors require thermal equilibrium to be achieved. This property increases the detection time required for measurements, and generally leads to lower responsitivity than coherent detectors. In addition, each thermal detector type has unique features that investigators must consider: cost, size, weight, spectral range, ease and temperature of operation, aperture size, damage thresholds, sensitivity (i.e. noise equivalent power (NEP) in $WHz^{-0.5}$, and response time (ms). In the following section, we provide a brief overview for each commonly used THz thermal sensor.

Calorimeters are ideal THz detectors for several reasons: (i) one of the few calibrated detectors (i.e. NIST-traceable) that permit absolute power measurements, which are required for laboratory standards studies; (ii) calorimeters typically have large apertures, high damage thresholds, high max power densities, and low noise levels (~10 μW); (iii)

large dynamic range typically from 3 mW to 30 W; and (iv) physical dimensions and operation: small, light, inexpensive, and operate at room temperature. The main drawback of calorimeters is their slow response time (typically, a few seconds).

Golay cells also exhibit several features that make ideal THz detectors: (i) broad operational range (0.1–10 THz); (ii) high sensitivity with low NEP values ranging from 10^{-8}–10^{-10} $WHz^{-0.5}$; and (iii) superior response time (typically, several ms) (iv) large dynamic range (~100 nW-1 mW); and (v) high responsivity (~10^4 V/W). The main drawbacks of Golay are their expense, large size, and low responsivity at higher THz frequencies.

Bolometers exhibit many properties that make them one of the most commonly used THz detectors for low power experiments: (i) ultrahigh sensitivity with NEP on the order of 10^{-11} to 10^{-17} $WHz^{-0.5}$; (ii) short response time, typically ranging from 50 ps to 1 ns; (iii) incredible sensitivity. The primary limitations of bolometers are the following: (i) require large crysostat systems to cool detectors to temperatures between 50 to 300 mK; (ii) broad dynamic range and sensitive to all types of energy and radiation; (iii) low maximum power handling capacity on the order of 1 mW.

Pyroelectric detectors are the most widely used ambient thermal detectors for several reasons: (i) broad operational range (0.1–30 THz); (ii) short response time, typically less than a second; (iii) high damage threshold (50 mW cm^{-2}); and (iv) user-friendly physical dimensions and operation: small, light, inexpensive, and operate at room temperature. Pyroelectric detectors have two main limitations. First, they provide relative power measurements, and therefore must be calibrated. Second, they have small aperatures, typically several mm in diameter, which often times is on the order of the THz beam diameter.

5.3 Equipment used for controlled exposures and accurate dosimetry

In order to ensure THz exposures are conducted in an accurate, controlled, and reproducible fashion, high quality *in vitro* THz biological studies employ several common elements. Perhaps, the most critical element is a temperature-controlled exposure chamber. Exposure chambers are either custom built using stainless steel or plexiglass materials, or they are designed using conventional cell culture incubators. Figure 5b and c contain images of a retrofitted chamber using a cell culture incubator, and a custom-designed exposure chamber, respectively [120, 145]. Chambers generally consist of an external heater, temperature controller, gas control and purging system, sapphire windows for IR measurements, operator control area, and input ports for THz radiation.

Exposure chambers serve several important purposes. First, they ensure that the biological samples are maintained under appropriate homeostatic conditions during THz exposures (typically, 37°C, 95% humidity, and 5% CO_2). Maintenance of homeostatic conditions is of paramount importance because mammalian cells can undergo stress responses when exposed to room temperature conditions. As a result, such conditions can lead to biological effects that may be artifacts. Thus, when exposure chambers are not employed, it becomes difficult to determine whether the observed biological effects are a direct result of the THz radiation or are due to the non-homeostatic environmental conditions. In addition to maintaining the exposure temperature, exposure chambers can also control the CO_2 levels. Controlling CO_2 levels is important because CO_2 levels are closely related to intracellular pH levels, which can dramatically affect the thermosensitivity of biological materials. Another reason exposure chambers are used in THz studies is that they provide a controlled-environment, which permits maximum THz delivery to the biological sample. In summary, exposure chambers are important systems for ensuring *in*

vitro THz bioeffects studies are performed in an accurate, controlled, and reproducible manner.

Temperature measurement devices are a second common element used in THz biological research studies. Such devices are used to measure the temperature rise generated in THz-irradiated biological samples. Temperature measurements are not only useful, but are actually required for accurate dosimetric calculations. The most common devices are thermistors, thermocouples, thermopiles, and fiber optic temperature sensors. These devices are frequently employed because they are fairly accurate, measure a wide range of temperatures, and are inexpensive. However, all of these devices suffer from the same limitation, which is that they each require direct contact with the target material. Direct contact can lead to appreciable measurement errors, which are most often due to direct optical absorption into the sensor, free space antenna effects, field perturbation, and inhomogeneity in biological materials.

Due to the limitations associated with contact temperature measurement devices, several noncontact approaches have been developed for estimating temperatures with high spatial resolution. The most common examples include IR thermographic imaging and Raman spectroscopic techniques. In brief, IR cameras estimate surface temperatures using the blackbody infrared emission of the sample, while Raman techniques rely on the recording of changes in the stretching band of the hydroxyl group in water at 3100 to 3700 cm^{-1}[146].

Computational M&S tools are the final common element employed in most THz studies. Computational M&S techniques are incredibly valuable tools, which are finding increased use in THz biological research. For example, these tools are commonly used to determine field distribution in biological materials, to calculate the expected temperature rise during THz exposures, and to predict tissue damage thresholds [121, 122, 147, 148]. There are many different types of modeling techniques, but the most commonly used methods are FDTD, Finite Element method (FEM), Finite Difference, and Monte Carlo. For further details we refer the reader to the following book [60].

5.4 Challenges and considerations for conducting terahertz biological research

In order to conduct high quality THz bioeffects studies, researchers must overcome numerous challenges and address several considerations. In the previous section, we provided an overview of THz sources, detectors, exposure chambers, and dosimetric tools. From this section, the following considerations were determined to be fundamental and should be reported in all studies: (i) exposure duration and THz irradiance incident on the biological sample or subject; (ii) characterization of THz beam quality; (iii) detailed specifications of detector: temperature of operation, aperture size, damage thresholds, NEP, and response time. (iv) use of gas- and temperature-controlled exposure chambers for *in vitro* studies; and (v) use of empirical and computational modeling dosimetric analysis.

In addition to the above considerations, there are several other experimental design and analysis elements that must be addressed. First, several experimental controls should be included in the design of THz experiments. These include negative controls (unexposed), sham exposed samples, and positive controls (heat, UV radiation). Ideally, thermal positive controls should be examined which use temperature-time histories that are matched to those of the THz-exposed samples. Second, the population size must be appropriate, ideally determined using conventional power analysis techniques. Third, all of the following experimental details should be provided: type of THz source, frequency, operation mode (CW or pulsed), exposure duration, irradiance, temperature of exposure chamber, and

dosimetric data. Finally, all samples should be coded such that the investigators are unaware of the status of the samples until all experiments and statistical analyses are completed. This approach reduces the investigator's bias during analysis.

6 Methodology and survey of the literature

For this review, we used several online search engines, including PubMed, Springer, Web of Science, and Google Scholar to identify experimental studies reported on the biological effects of THz radiation. Relevant studies published on or before March 2011 were selected from peer-reviewed journals, book chapters, proceedings, and meeting abstracts. In addition, we analyzed the project summaries for the "THz-BRIDGE" project–the first international THz biological research project [149]. We also examined more recent work initiated by the German Federal Office for Radiation Protection (Bundesamt für Strahlenschutz – BfS) [150] and the THz-BEAM projects. We also searched for relevant publications in the journal entitled "Bulletin of Experimental Biology and Medicine." We mined this particular journal because it contains the English version for many studies originally published in Russian. Additionally, we also included an analysis for studies which were only published in Russian and Chinese. Translations for these works were kindly provided by corresponding authors.

After surveying the literature, we identified a total of 46 empirical studies. In order to provide a historical perspective on trends in this field, we classified each study by the year of publication, type of THz source, frequency range, and biological model (Fig. 6). The data indicates that roughly 50% of the studies used FIR sources, 13% FELs, 13% klystron or BWO sources, 9% optical sources (typically Ti-Sapphire and photoconductive antennas), and 17% electronic sources (microwave generators or other frequency upconversion sources (Fig. 6a). The data also shows that the sources used most often in recent years are FIR lasers, FELs, and electronic sources.

Figure 6b contains a plot of the frequency range examined in each study. The data shows that roughly 40% of the studies examined effects at low THz frequencies (0.1–0.15 THz), and roughly 40% examined effects at higher THz frequencies (2.0–7.0 THz). Interestingly, few studies have been performed at frequencies greater than 7 THz or for frequencies between 0.15–2.0 THz. The data also shows that recent studies have continued to focus on both the low and middle THz frequency ranges.

Figure 6c is a plot of the type of biological system used in each study. The data indicates that 13 publications were reported before 1996, and 32 were published after 1996. The data also shows that most THz studies have been performed on cell cultures (40%) and on isolated biological macromolecules: protein (11%), DNA (9%), and organelles (9%). The timeline suggests that in recent years research groups are conducting more *in vivo* studies using human subjects, rats, and mice. In the next section we shall provide a comprehensive study-by-study analysis of each study.

6.1 Comprehensive study-by-study analysis of terahertz bioeffects studies

6.1.1 In vivo studies on organisms: vertebrates (humans, rats, and mice), insects, and plants

Human subjects

Study 1. To date, the only THz bioeffects study performed on human subjects was reported by Ostrovskiy *et. al.* in 2005 [151]. In this work, the authors postulated that THz radiation

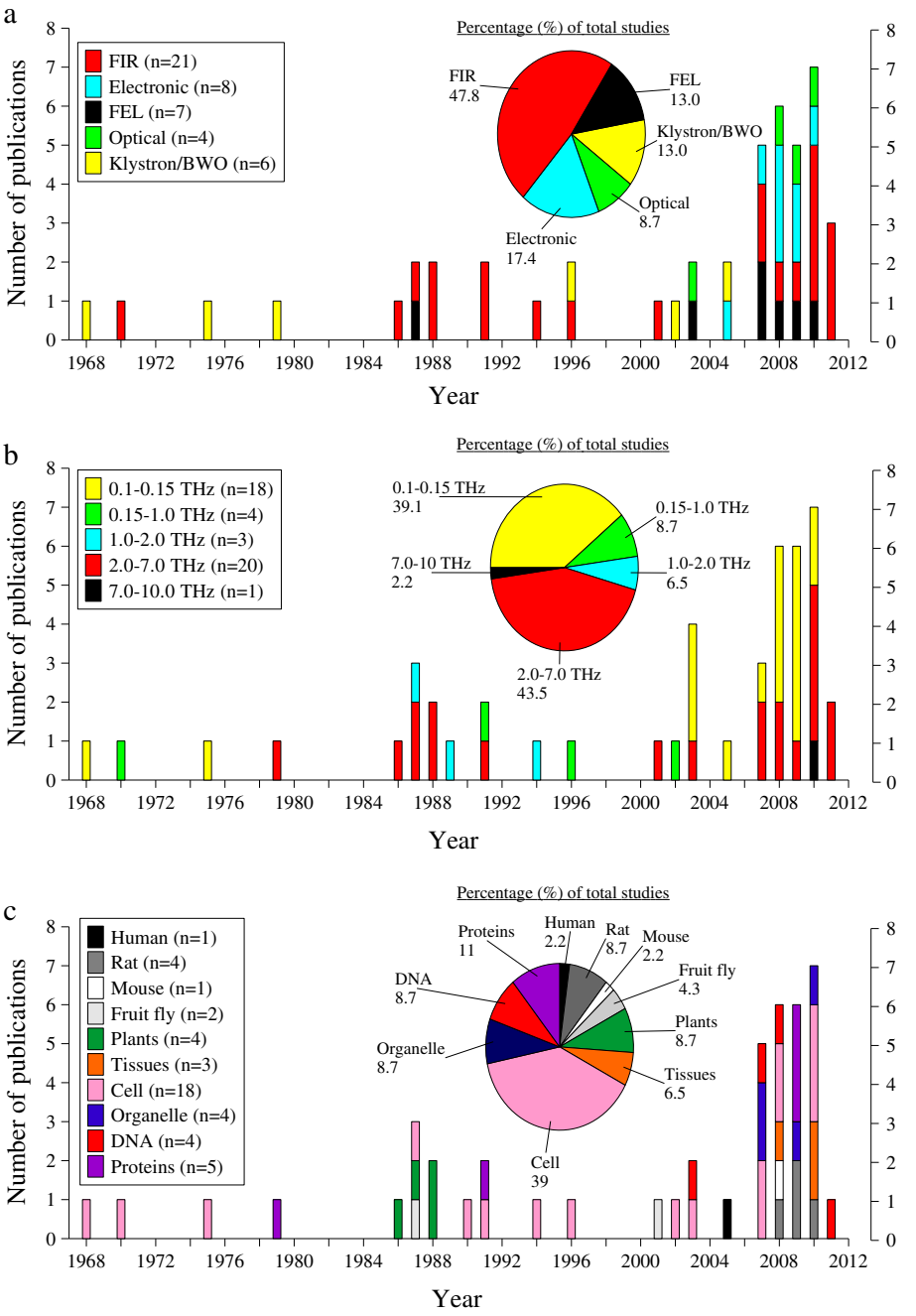

Fig. 6 (**a**–**c**) THz biological research studies: Analysis and trends. **a**. THz sources: number of publications using each source type plotted versus year. **b**. THz frequency range: number of publications for each frequency range plotted versus year. **c**. Biological system: number of publications for each biological model type plotted versus year. Percentages of total publications are provided as pie charts as insets for each plot.

may be a useful treatment for burn repair and microbial dissemination. To test this hypothesis, the authors treated patients suffering from superficial and deep burns (n=14 and n=21, respectively) with THz radiation: 0.15 THz, 0.03 $mWcm^{-2}$, 15 minute treatments, and 7–10 treatments per day. (Table 1). The results of this work indicate that THz treatments enhanced the repair of localized burns by accelerating the epithelialization process. In addition, THz treatments were shown to increase microbial dissemination in deep burns by 100 to 1000 fold. Unfortunately, empirical dosimetric data is not provided in this study, but our computational models (described in [120]), predict that the THz-induced temperature rise is roughly 0.1°C. Figure 7a contains a plot with the temperature and exposure time for these exposures and conventional thermal effects. Since these exposures result in small temperature rises, thermal mechanisms are most likely not responsible for the observed effects. The authors suggest that the effects are due to the strong absorption of nitric oxide (NO) molecules at THz frequencies. In summary, this study provides evidence that THz radiation may be a useful therapy for burn care.

Rats (Rattus norvegicus)

Study 1. In 2008, Kirichuck *et al.* conducted the first *in vivo* THz bioeffects study on a rat model [152]. The authors hypothesized that THz radiation may elicit effects on the functional activity of platelets. They further postulated that such effects may be sex-specific, and may be the result of the preferential interaction of THz radiation with female hormones. To test this hypothesis, the authors exposed male and female rats (n=15) to THz radiation using a microwave generator: 0.15 THz, 0.7 mW, 0.2 $mWcm^{-2}$, and 15 or 30 min exposures (Table 1). Three hours post-exposure, platelet-rich plasma samples were collected and evaluated using a platelet aggregation analyzer. Data was analyzed using several statistical tests, including Shapiro-Wilks and Mann-Whitney tests. Results from this study indicate that both male and female exposed rats exhibited complete recovery of platelet aggregation. Data also showed that female rats were more sensitive to the treatment. The authors suggest that the selective absorption of metabolites (NO, O_2, CO_2, CO, OH^-) at 0.15 THz may contribute to the observed effects. Empirical dosimetric data is not provided in this work, but our computational models indicate the temperature rise during treatments is less than 0.1°C (Fig. 5). The authors presume that the observed effects are not mediated via thermal mechanisms.

Study 2. Similar to their 2008 work, Kirichuk *et al.* conducted a second study to investigate whether THz irradiated albino rats exhibited both enhanced platelet aggregation and behavioral alterations (i.e. depression) [153]. To test this hypothesis, rats were exposed to THz radiation using a microwave generator: 0.15 THz, 3 $mWcm^{-2}$, and exposure durations of 15, 30 or 60 min (Table 1). Platelet aggregation was evaluated as described in [152], and rat behavior was examined using a maze designed to test for depression. Experiments were carried out on 75 male rats, 15 controls, and 60 experimental stress immobilized rates. Several evaluation parameters were assessed using statistical analysis tools: total test time, total number of entries and exits, and number of peepings at various positions in the maze. The results of this study indicate that rats exposed to THz radiation for 60 min exhibited increased levels of depression and enhanced platelet aggregation. Interestingly, rats exposed to durations shorter than 60 min did not exhibit either effect. Empirical dosimetric data is not provided in this study, but our computational models predict that the temperature rise is less than 0.1°C. Appreciable thermal effects are typically not observed for matched thermal exposures, thus, the mechanisms responsible for the observed effects remains unclear (Fig. 7a).

Study 3. Last year, Kirichuk *et al.* hypothesized that THz radiation may be useful for restoring lipoperoxidation (LPO) processes and antioxidant activity in rats suffering from

Table 1 Summary of THz studies at an organism and tissue level. Measurements not conducted in the study are denoted with an (*). Values with insignificant differences are denoted (NS). Temperatures in parentheses are predicted using computational simulation dosimetric models [120].

STUDY TYPE Model	THz source	THz frequency	CW or Pulse	Duration (Minutes)	Φ (mW/ cm^{-2})	ΔT rise (°C)	Behavioral effects	Systemic, Tissue, Cellular effects	Citation: (Author year), [#]
HUMAN									
in vivo human subjects	Electronic (Gunn)	0.15	CW	15,30	0.02–0.03	(≤0.1)	*	+ epithelialization, + microbial dissemination	(Ostrovskiy *et al.* 2005) , [151]
RAT									
in vivo white rats	Electronic (Gunn)	0.129	CW	5–30	0.1	(≤0.1)	*	+ coagulation & fibrinolysis	(Kirichuk and Tsymbal 2010) , [155]
in vivo male albino rats	Electronic (Gunn)	0.15	CW	15–60	3.0	(~0.1)	+ depression	+ platelet aggregation	(Kirichuk 2009) , [153]
in vivo male albino rats	Electronic (Gunn)	0.15	CW	15,30	0.2	(≤0.1)	*	+ lipoperoxidation & antioxidants	(Kirichuk and Tsymbal 2009) , [154]
in vivo male & female albino rats	Electronic (Gunn)	0.15	CW	15,30	0.2	(~0.1)	*	+ platelet aggregation: ↑ in females	(Kirichuck *et al.* 2008) , [152]
MOUSE									
in vivo male mice (C57B1/6 J)	FIR	3.6	CW	15–30	23.6	(2.0)	+ anxiety	*	(Bondar *et al.* 2008) , [156]
FRUIT FLY									
in vivo D.melanogaster (fruit fly)	FIR	2.5 & 6.69	CW	90–150	3.18 & 0.95	(≤0.5)	*	+ induction of protein expression	(Hu 1987) , [158]
in vivo D.melanogaster (fruit fly)	FIR	3.68	CW	60	30	(~1.25)	*	+ affect on somatic mutations induced by γ-radiation	(Federov 2001) , [159]
PLANTS									
in vivo paddy rice	FIR	2.5 & 6.69	CW	10,20,30	3.18 & 0.95	(≤0.5)	*	+ stimulation of growth	(Xiong and Shaomin 1986) , [160]
in vivo black beans	FIR	2.5 & 6.69	CW	15,30,45	3.18 & 0.95	(≤0.6)	*	+ stimulation of growth	(Peng 1987) , [160]
in vivo wheat	FIR	2.5	CW	30	1.0	(≤0.1)	*	+ stimulation of growth & esterase activity	(Xu and Xiong 1988) , [162]
in vivo paddy rice	FIR	2.5 & 6.69	CW	10,20,30	3.18 & 0.95	(≤0.5)	*	+ induction of chlorophyll mutations	(He and Su 1988) , [163]
TISSUES									
Chamois cloth	FEL (JLabs)	0.1–1.0	CW	0.033	2000–14000	35	*	+ tissue damage threshold	(ED50) = 7160 mW/cm2 (Dalzell *et al.* 2010) , [122]
Excised porcine skin & egg whites	FIR	1.89	CW	60	181.9	10–12	*	+ visible coagulation observed on several samples	(Dalzell *et al.* 2010) , [122]
in vitro human blood with isoket	Electronic (Gunn)	0.24	CW	15	1.0	(~0.1)	*	+ reduced blood viscosity &+erythrocyte deformability	(Kirichuk *et al.* 2008) , [164]

immobilization stress [154]. The authors tested this hypothesis by exposing male albino rats to immobilization stress using a supine fixation technique. Rats (n=75) were then randomized into several groups: control, immobilized and not THz irradiated, immobilized and THz irradiated (15 min), immobilized and THz irradiated (30 min). THz treatments were delivered with the source described in [153] using the following parameters: 0.15 THz, 0.7 mWcm^{-2}, and 15 or 30 min exposure durations (Table 1). After exposures, blood was extracted and evaluated using several indices for LPO and antioxidant levels: lipid hydroperoxides, SH-groups, SOD, and vitamin E. The results of this study indicate that rats exposed to THz radiation for 30 min exhibited statistically significant changes in several intermediate products of LPO and blood antioxidant activity. Empirical dosimetric data is not provided in this study, but our modeling data predicts that the temperature rises are less than 0.1°C. Such exposures are not expected to cause any significant heat-induced biological effects (Fig. 7a). The authors propose that the selective absorption by NO molecules at 0.15 THz is partly responsible for the observed effects.

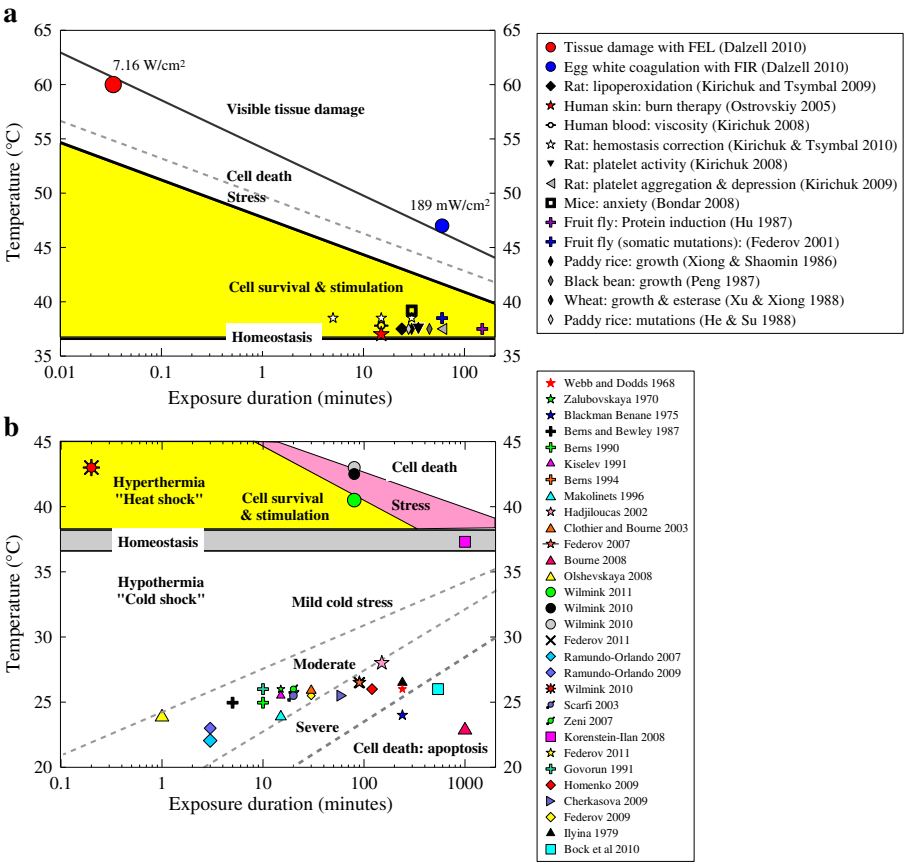

Fig. 7 (**a**–**b**) Summary plot of published THz studies reporting on the biological effects at an organism, tissue, cellular, organelle, and biological macromolecular level. For a reference, conventional pathologic thermal effects data are also provided for various heating regimes (temperature-time).

Study 4. The most recent study using a rat model was performed earlier this year [155]. In this work, the authors postulated that THz radiation may be an effective therapeutic tool for the treatment of hemocoagulation and/or fibrinolysis dysfunction of rats suffering from immobilization stress. To test this hypothesis, the authors exposed the skin of mongrel white rats to THz radiation using a microwave generator source and a similar immobilization stress procedure as described in Kirichuck *et al.* [154] . The following exposure parameters were used: 0.129 THz, 0.1 $mWcm^{-2}$, and exposure durations of 5, 15, or 30 min. Blood was collected post-exposure, and evaluated using a solar turbidimetric hemocoagulator. Several coagulation and fibrinolytic properties were assessed: activated partial thromboblastin time; international normalized ratio; fibrinogen concentration; thrombin clotting time, and factor XIII activity. The data indicates that 5 minute exposures did not cause an effect on the evaluated parameters; however, both the 15 and 30 minute exposures induced normalization effects on both coagulation and fibrinolysis markers. Empirical temperature data was not collected in this work, but our M&S models predict skin temperature rises of less than or equal to 0.1°C for the 30 min exposures. Given the thermal bioeffects data provided in Fig. 7a, these tissues exposed to matched temperature rises typically do not exhibit appreciable biological effects. In summary, although the exact mechanism for the effects observed in this study is not clear, this work provides evidence that THz radiation may show promise as a useful clinical tool for normalizing coagulation and fibrinolysis dysfunction.

Mice (Mus musculus)

Study 1. To date, the only THz bioeffects study performed on mice was conducted in 2008 by Bondar *et al.* [156]. Similar to their work where they used a rat model [153], this group postulated that THz radiation exposures may cause behavioral effects (i.e. anxiety) in mice. To test this hypothesis, the authors exposed mice (n=10–12) to THz radiation: 3.6 THz, 23.6 $mWcm^{-2}$, and exposure durations of 15 or 30 min. The behavior of the mice was evaluated post-exposure using an elevated "plus-maze" designed to test for anxiety. Several parameters were quantified and analyzed with Mann-Whitney statistical approaches: total test time, total number of entries and exits, and number of peepings at various positions in the maze. The data from this study show that mice exposed to THz radiation for 15–30 min exhibited increased levels of anxiety. The authors reported that the mechanism and physiological responses responsible for these effects is "unclear." Given the difficulty in collecting temperature data on mobile mice, empirical dosimetry was not conducted in this study. However, we used our computational models to predict the temperate rise for a mouse receiving direct exposure to THz radiation for 30 min. (Note: the angle of irradiation, specular loses, and the curvature of the mouse body were considered in these calculations). Our data indicates that a maximal temperature rise of roughly 2°C is expected for the 30 min exposure. Although, this temperature rise is greater than in the rat studies, appreciable thermal effects are typically not observed for matched heating exposures.

6.1.2 Insects: Fruit fly (Drosopholia melanogaster)

Study 1. In the late 1980s, Hu *et al.* conducted the first THz bioeffects study using a fly model [157, 158]. The authors hypothesized that THz radiation may cause genetic mutations in flies. To test this hypothesis, pupae and adult flies were exposed to THz radiation using an FIR laser. The following exposure conditions were employed: (i) 2.5 THz, power = 10 mW, H=3.18 $mWcm^{-2}$; (ii) 6.69 THz, power =1 mW, and H= 0.95 $mWcm^{-2}$ (Table 1). All exposures were conducted for 90–150 min. The protein

expression of the flies was examined post-exposure using electrophoresis gels. The results of this work indicate that both frequencies of THz radiation affect the gene expression in flies, and that these effects were most pronounced at 6.69 THz. Interestingly, using computational dosimetric models, we predict that both the 2.52 THz and 6.69 THz treatments would induce temperature rises in the flies of roughly 0.5°C for the 150 min exposures. Given the thermal bioeffects data provided in Fig. 7a, the thermal history provided by these exposures is not expected to denature proteins and/or elicit CSR mechanisms in mammalian cells; however, comparable hyperthermic studies in a fly model have not been published to date.

Study 2. Ten years ago, Federov *et al.* conducted a series of experiments to investigate the effects that IR and THz radiation have on fly mutation rate [159]. In this work, the authors exposed adult larvae flies (n=40–100) to THz radiation using a FIR THz laser source: 3.69 THz, 30.0 $mWcm^{-2}$, and exposure duration of 60 min (Table 1). The authors report that larvae exposed to THz radiation enhanced the number of somatic mutations observed in flies, which were pre-exposed to gamma-radiation. Using computational dosimetric models, we predict that both of these exposures would generate temperature rises of roughly 1.25°C for the 60 min exposures (Fig. 7a).

6.1.3 Plants: Rice paddies, black beans, and wheat

Study 1. In the mid-1980s, Xiong *et al.* examined the effects of THz radiation using a rice paddy model [157, 160]. In this study, the authors hypothesized that THz radiation may directly affect cell growth, resulting from the excitation of the electric modes of biomolecules. To test this hypothesis, the authors exposed paddy rice to THz radiation using the same source described in Hu *et al.* [157, 158]. The following exposure conditions were employed: (i) 2.5 THz, power = 10 mW, H=3.18 $mWcm^{-2}$; (ii) 6.69 THz, power =1 mW, and H=0.95 $mWcm^{-2}$ (Table 1). Exposures were conducted for 10, 20, or 30 minutes. The rice paddies were assessed using the following criteria: breeding speed, rate of emergence, quality of rice seedlings (i.e., number of green leaves, width of stem, and number of tiller), period to turn green, length of growing period, and number of grains per stem. The experimental results of this work are the following: (i) breeding speed increased by 16–32% for 2.52 THz and 14–30% for 6.69 THz; (ii) rate of emergence increased by 12–20% for 2.52 THz and 10–18% for 6.69 THz; (iii) quality, number of green leaves, width of stem, and number of tiller all improved; (iv) period to turn green is shortened by 1.5–2.0 days; (v) growing period reduced by 4–5 days; (vi) number of grains per stem increased 15–28%. The authors conclude that the THz radiation can simulate the growth of rice plants. Experiments were not conducted to examine the mechanism responsible for these effects, but the authors suggest that the direct excitation of biomolecules may be a contributing factor. Interestingly, using our computational dosimetric models, we predict that both the 2.52 THz and 6.69 THz treatments would induce temperature rises in the rice paddies $\leq$0.5°C for the 30 minute exposures.

Study 2. One year after conducting their initial study [157, 160], Peng *et al.* conducted a similar study on black beans [161]. In similar fashion, the authors hypothesized that THz radiation can affect the breeding of black beans. To test this hypothesis, the authors exposed black beans to the same THz radiation exposure parameters used in [157, 160]. One difference between the studies is authors used longer exposure durations (15, 30, or 45 minutes). Black beans were evaluated using the following markers: rate of seedling emergence, initiation of budding, number root nodules, number grains per stem, and length of growing period. The experimental results were the following: (i) rate of seedling

emergence increased by 8–12%; (ii) budding occurred 2–3 days earlier; (iii) number of root nodules increased by 2.15 for 2.52 THz and 2.27 times for 6.69 THz; (iv) number of grains per stem increased by 25%; (v) complete growing period was unchanged, lengthened, and shortened according to exposure duration. Similar to the rice study, the authors conclude that the THz radiation can simulate black bean growth. Interestingly, using our computational dosimetric models, we predict that both the 2.52 THz and 6.69 THz treatments would induce temperature rises in the black beans $\leq$0.6°C for the 45 minute exposures. Given the thermal bioeffects data provided in Fig. 5, these exposures are not expected to cause any significant biological effects.

Study 3. In their final published report, Xu and Xiong *et al.* examined the effect of THz radiation on the growth, breeding, and esterase distribution of wheat [157, 162]. The same THz source and exposure parameters were employed as described in Hu *et al.* [157]; however, a lower irradiance (1 mW/cm^2) and a shorter exposure duration (30 minutes) were used. The experimental results were the following: (i) for 2.5 THz and 6.69 THz the rate of seedling emergence increased by 21% and 16%, respectively; (ii) rate of survival increased by 18% and 20%, respectively; (iii) stem height, length of ear, numbers of ears, grains, and produce per stem, were all increased; (iv) reduced sterility; (v) increased levels of esterase activation and activity increased by 13–20%. The authors concluded that THz radiation may mediate its effects on wheat growth via direct modulation of esterase activity.

Study 4. In the late 1980s, He and Su *et al.* employed a paddy rice model to examine the effect that THz radiation has on chlorophyll mutations [157, 163]. In this study, they irradiated paddy rice to THz radiation for 10, 20, and 30 min (as described in Hu *et al.* [157]). Mutations were observed for all exposures, but the highest rate of mutation was observed for the 30 min exposures at 6.69 THz. Definitive experiments were not conducted to elucidate the mechanism responsible for these effects, but the authors believe that the direct excitation of biomolecules may be a contributing factor. The dosimetric data we computed using our computational models predicts that both the 2.52 THz and 6.69 THz treatments would induce temperature rises in the paddy rice that is less than 0.5°C for the 30 min exposures. Given the thermal bioeffects data provided in Fig. 7a, these exposures are not expected to cause any significant thermal effects in tissues or cells.

6.2 *Ex vivo* studies on excised skin tissues and blood (specialized connective tissue)

Study 1. In early 2010, Dalzell *et al.* used computational modeling and experimental approaches to determine tissue-damage thresholds at THz frequencies for both short (several seconds) and long duration exposures (min) [122]. For the short exposure studies, wet chamois clothes were irradiated using the FEL at Jefferson Laboratory: 0.1 to 1.0 THz, 2.0 to 14.0 Wcm^{-2}, and a 2s exposure duration. For the long exposure studies, freshly excised porcine skin and egg whites were exposed using a FIR THz laser: 1.89 THz, 189.92 mWcm^{-2}, and 60 min duration. Computational modeling tools using an Arrhenius damage model were used to predict damage-thresholds. Thresholds were also empirically determined using conventional damage score determination and probit analysis techniques. Empirical dosimetery was performed for exposures using IR cameras and thermocouples.

For the short duration experiments, the tissue damage threshold (ED50) was determined to be 7.16 Wcm^{-2}, and the final tissue temperature was shown to be 60°C. As expected, the data shows that increases in incident irradiance Φ resulted in linear increases in final tissue temperatures. For the longer duration experiments using lower irradiances, the irradiated excised porcine samples did not exhibit signs of tissue damage; however, several egg white samples showed visible signs of coagulation. The dosimetric data shows that the

temperature of the egg whites increased between 10–12°C during the 60 min exposures. These data points are both within the damage regions that are associated with visible tissue damage (Fig. 7a).

Study 2. Kirichuk and Androvov *et al.* conducted a study to determine if THz radiation therapies could be used to treat patients with unstable angina (chest pain) [164]. THz radiation is known to be strongly absorbed by NO; therefore, the authors hypothesized that THz treatments may be useful for the correction of blood rheology parameters. To test this hypothesis, the authors collected whole blood from normal healthy patients (n=150) and patients suffering from unstable angina (n=60). Blood samples were treated with Isoket (nitrate vasodilator drug) and with THz radiation (0.24 THz, 1 mW/cm^2, 15 minute duration) (Table 1). The effects of the treatment were evaluated post-exposure using several blood rheology parameters: viscosity, aggregation, and erythrocyte deformability. The results of this work indicate that THz-irradiated isokets exhibited a reduction of blood viscosity, no effect on erythrocyte aggregation, and an increase in erythrocyte deformability. The authors conclude that THz radiation may be a feasible treatment for patients suffering from unstable angina. Practically speaking, such an application would likely require fiber optics probes to directly deliver the THz energy to the blood. Temperature data was not measured in this study, but our computational models indicate that the exposures would generate negligible temperature rises (Fig. 7). As a result, the effects observed in this work do not appear to be caused by macroscopic bulk heating effects.

6.3 *In vitro* studies using mammalian cells

Study 1. In 1968, Webb *et al.* conducted the first study to examine the effect of THz radiation on cellular systems [165]. In this work, they examined the effects of THz radiation on *E. coli* cell growth. Exposures were performed with a Kylstron source using the following parameters: exposure temperature (25°C), 0.136 THz, H=0.22 mWcm^{-2}, exposure durations of 30–240 min (Table 2). Microcolony growth areas were evaluated post-exposure using time-lapse photographic techniques, and temperatures were predicted for each exposure. The results of this study indicate that THz radiation inhibited the growth of *E.coli* cells. The observed effects increased with exposure duration, where the 150 minute and 240 minute exposures reduced cell growth by two-fold and seven-fold, respectively. The authors observed a 1°C temperature rise during exposures (Fig. 7b). Interestingly, mammalian cells exposed to temperatures of 26°C for greater than 100 min typically undergo “cold shock”, which is reported to affect cell growth [166]. Therefore, the cold shock conditions may have partly contributed to the observed reduction in cell growth.

Study 2. Zalyubovskaya *et al.* conducted the first *in vitro* cell culture study exploring the effect that THz radiation has on several different human cell lines[167]. In this work, exposures were conducted using a FIR THz source using the following parameters: exposure temperature (25°C), 0.89 THz, H=0.3–1.0 mWcm^{-2}, 15 minute exposure durations (Table 2). The authors exposed HeLa, Hep-2, and RH cell lines. In all cell lines, the authors observed several effects: destruction of cell membrane, an appearance of multinuclear cells, an increase in nuclear size, increase in cytoplasm granularity, and increased cell death. Temperature data was not collected in this study, but our computational models predict that the rise in temperature is roughly would be 1°C during the exposures (Fig. 7b). The authors suggest that all of the effects are a consequent of the direct interaction of THz radiation on lipid membrane and DNA.

Study 3. In 1975, Blackman *et al.* conducted an *in vitro* study in an attempt to replicate the work conducted by Webb *et al.* [165]. The authors used the same cell lines, THz source,

and evaluation criteria as described in Webb [165] (Table 2). In contrast to the results observed in Webb *et al*., Blackman reported that THz radiation did not cause any appreciable effects on cell growth.

Study 4. Berns and Bewley *et al.* investigated the effect that 1.5 THz radiation has on DNA synthesis in rat kangaroo kidney epithelium cells lines (PtK2)[142]. Experiments were conducted on cells at room temperature (25°C) using the FEL at UCSB. The exposure parameters were the following: 1.5 THz, 2 μs pulse length, 2.6 mJ per pulse, beam radius 0.4 cm, 10–100 total pulses, 6s between pulses, 100 W/cm^2, average power of 0.1 mW/cm^2, and exposure durations of 1–10 min (Table 2). Cellular morphology and DNA synthesis of the cells were examined using [^{3}H] thymidine isotopes, standard light microscopy, and autoradiographic analysis techniques. Temperatures were not measured during exposures, but the authors used computational methods to predict the temperature rise during irradiation. The data shows that 7% of the THz-exposed cells exhibited signs of cell death. Additionally, morphological changes were observed immediately (30 minutes) post-exposure. The DNA synthesis results show that 17% of cells exposed to 100 pulses scored positive for "light" [^{3}H] thymidine staining, compared to only 11% of control cells. This data suggests that THz-exposed cells exhibited statistically significant increases in inhibition of DNA synthesis. The authors conducted several additional studies to investigate the mechanism for these effects, and concluded that the target is not the lipid membrane but rather DNA. The authors predicted that the temperature rise during exposures was 2.96°C (Fig. 7b).

Study 5. In 1990, Berns and Bewley *et al.* conducted a follow-up investigation to their 1987 study [140]. In this work, they further hypothesized that THz radiation may elicit varied effects on the inhibition of DNA synthesis in synchronized versus asynchronized cells. To test this hypothesis, they exposed both synchronous and asynchronous Chinese hamster ovary (CHO) cells (*Cricetulus griseus*) to THz radiation. They employed the same FEL source as described in their previous work [142]; however, the exposure parameters were slightly different: 1.5 THz, 2 μs pulse length, repetition rate of 0.5–0.33 Hz, 2.6 mJ per pulse, beam radius of 0.0135 cm, 100 total pulses, 1.3 kW/pulse, and exposure duration of 5 min (Table 2). The authors used the same DNA analysis techniques described in [142]. The data indicates that synchronous and asynchronous THz-exposed cells both exhibited inhibition in DNA synthesis. In line with their hypothesis, synchronous cells exhibited higher levels of inhibition than the asynchronous cells, 22% versus 17%, respectively. During these short exposures, the authors predicted that the maximum temperature rise during THz irradiation was 2.96°C (Fig. 7b). The authors conclude that the observed effects are likely not "thermally mediated."

Study 6. In 1991, Kiselev *et al.* evaluated the effects of THz radiation on the cellular production of hemolysins in rats immunized with staphylococcal vaccine [168]. The authors isolated immunocompetent spleen cells from the spleen of the rats and then studied the effect that THz-exposed staphylococcal corpuscular antigens have on the production of hemolysins—substances produced by staphylococci bacteria that lyse red blood cells. Exposures were conducted using a FIR THz source using the following parameters: exposure temperature (25°C), 0.89 THz, H=0.06–0.25 mWcm^{-2}, and 15 min duration (Table 2). The authors observed that the THz exposures using lower irradiances (0.06–0.125 mWcm^{-2}) induced moderate stimulation of hemolysins production by rat spleen cells, whereas higher irradiances (0.25 mWcm^{-2}) caused a decrease in production. The authors report that the mechanism responsible for this "window" effect is not clear. In addition, although the authors do not report temperature measurements, our computational models predict that the temperature rise is less than a 1°C during exposures (Table 2).

Table 2 Summary of cellular effects associated with THz radiation. Measurements not conducted in the study are denoted with an (*). Values with insignificant differences are denoted (NS). Temperature data predicted with computational models is in parentheses

Biological system	THz Source	Frequency (THz)	CW or Pulsed	Duration (Minutes)	Φ ($mWcm^{-2}$)	Exposure Temp.(°C)	ΔT rise (°C)	Cell death (%)	Growth, migration, morphology, adhesion	Lipid membrane	Protein expression, conformation, or recognition	DNA	Citation: (Author year), [#]
Cellular													
E.coli cells	Klystron	0.136	CW	30–240	0.22	25	<1	Not lethal	↓ growth	*	*	*	(Webb and Dodds 1968), [165]
Hela, Hep2, RH	FIR (HCN)	0.89	CW	15	1.0	25	(<1)	observed	+ morphology	destruction	↓ immune res.	*	(Zalyubovskaya *et al.* 1970), [167]
E.coli cells	Klystron	0.136	CW	30–240	0.22	25	(≤1)	*	NS	*	*	*	(Blackman *et al.* 1975), [184]
PTK2	FEL (UCSB)	1.50	0.5 Hz	1–10	0.5–4.0 kW/p	22	2.96	7%	*	*	*	↓ synthesis	(Berns and Bewley 1987), [142]
CHO	FEL (UCSB)	1.50	0.5 Hz	5	1.3 kW/p	22	2.96	*	*	NS	*	↓ synthesis	(Berns *et al.* 1990), [140]
Rat spleen cells	FIR (HCN)	0.89	CW	15	0.4	25	(<1)	*	*	*	↑ IgG production	*	(Kiselev 1991), [168]
CHO,PTK2	FEL (UCSB)	1.50	0.5 Hz	5	5 1.3 kW/p	18	2.96	*	*	NS	*	↓ synthesis	(Berns *et al.* 1994), [141]
Rat spleen cells	FIR (HCN)	0.89	CW	15	0.13–0.25	25	(<1)	*	↑ migration	*	↓ immune res.	*	(Makolinets 1996), [169]
Yeast cells	BWO	0.34	CW	30–150	5.8	25	2–3	*	↑	*	*	*	(Hadjiloucas *et al.* 2002), [170]
NHK cells	TiS (PC Ant.)	1.0–2.7	80 MHz	10, 20,30	10	25	(≤1.0)	NS	↑ proliferation	NS	*	*	(Clothier and Bourne 2003), [19]
Red blood cells	FIR: NH_3	3.68	CW	30	20.0	25	(≤1.5)	*	↑ proliferation	↓ osmotic res.	*	*	(Federov 2007), [170]
Lymphocytes	FIR: NH_3	3.68	CW	90	20.0	25	(≤1.5)	38%	↑ proliferation	*	*	↑ synthesis	(Federov 2007), [170]
NHK/C, ND7/23	TiS (PC Ant.)	0.14–0.15	80 MHz	10–1440	62 (peak)	22	(≤1.0)	NS	NS	NS	NS	*	(Bourne *et al.* 2008) , [172]
Neurons	FEL (NOVO)	0.7, 2.5, 3.49	CW	1	0.3–30.0	22	(≤2)	*	All observed	disruption	morphological	*	(Olshevskaya *et al.* 2008), [20]
Fibroblasts	FIR (CH_3OH)	2.52	CW	80	81.5	37	3.0	10%	NS	NS	↑ stress proteins	NS	(Wilmink *et al.* 2010), [119]
Jurkats	FIR (CH_3OH)	2.52	CW	40	227.0	37	6.0	62%	↓	*	*	*	(Wilmink *et al.* 2010), [120]
Fibroblasts	FIR (CH_3OH)	2.52	CW	80	227.0	37	6.0	apoptosis	*	*	↑ stress proteins	↑ DNA repair	(Wilmink *et al.* 2010), [121]
Mouse stem cells	Freq-double	Broad, ~10	1 kHz	120–540	1	26.3	0.3	*	NS	Lipid droplets	↑ PPARG	*	(Bock *et al.* 2010), [106]
Fibroblasts	FIR: NH_3	3.68	CW	30–90	20.0	25	(≤1.5)	NS	*	*	NS	*	(Federov 2011), [173]
Organelle													

Liposomes	cFEL	0.13	2, 5, 7 Hz	2–3	5–17.0	22	0.03	*	*	↑ permeability	*	*	(Ramundo-Orlando *et al.* 2007), [18]
Liposomes	IMPATT	0.15	CW	2–3	6.2	22	0.05	*	*	NS	*	*	(Ramundo-Orlando *et al.* 2007), [18]
Liposomes	cFEL	0.15	2, 5, 7 Hz	2–3	1–3 kV/cm	22	0.05	*	*	↑ permeability	*	*	(Ramundo-Orlando 2009), [176]
Fibroblasts	FIR (CH_3OH)	2.52	CW	0.2	227.0	37	6.0	apoptosis	*	↑ permeability	↑ stress proteins	↑ DNA repair	(Wilmink *et al.* 2010), [121]
Biomolecules													
DNA													
Lymphocytes	FEL (ENEA)	0.12–0.13	2 Hz	20	1.0	25	(≤0.5)	NS	NS	NS	*	*	(Scarfi *et al.* 2003), [17]
Lymphocytes	FEL (ENEA)	0.12–0.13	2, 5, 7 Hz	20	0.05–0.23	23	0.35	*	NS	NS	*	NS	(Zeni *et al.* 2007), [16]
Lymphocytes	Electronic	0.10	CW	1440	0.031	37	0.3	*	+ replication	*	*	Aneuploidy	(Korenstein-Ilan *et al.* 2008), [15]
Lymphocytes	FIR (NH_3)	3.68	CW	10, 30, 60	20.0	25	(≤1.5)	*	*	*	*	Conformation	(Federov 2011), [173]
Enzymes													
Peroxidase, Albumin, OHD	FIR (NH_3)	3.33	Pulsed	*	0.6 J/ pulse	(≤0.5)	*	*	*		↓ enzymatic act.	*	(Govorun *et al.* 1991) , [180]
Trypsin					0.2-3 J						structural changes		
											↓ enzymatic act.		
Phosphatase	Electronic	0.1	CW	60–120	0.08	25	(≤0.5)	*	*	*	↓ recognition	*	(Homenko *et al.* 2009) , [14]
Albumin (BSA)													
BSA	FIR (NH_3)	3.60	CW	60	10.0	25	(≤0.5)	*	*	*	conformation	*	(Cherkasova *et al.* 2009) , [22]
BSA	TiS (PC Ant.)	0.12–13	80 MHz	30	10.6 μJ/ pulse	25	(≤0.5)	*	*	*	conformation	*	(Fedorov 2009) , [181]
Hemoglobin (Hg)													
Hg bonds	BWO	2.65 &3.33	CW	240	3.0	25	(≤0.5)	*	*	*	Strength Hg bond	*	(Il'ina 1979) , [136]

Pulsed[1] – parameters of laser radiation see in Batanov *et al.* Int.J. Infrared and Millimeter Waves 1990, v.11, p.435–442

FEL, Free electron laser; UCSB, University of California at Santa Clara; NOVO, Novosibirsk; ENEA, Research Center in Frascati, Italy; cFEL, compact FEL; FIR, Far infrared or optically-pumped THz source; freq-double, frequency doubling; IMPATT, impact ionization avalanche transit-time devices; TiS PC Ant, Titanium sapphire excitation of photoconductive antenna.

Study 7. In 1994, Berns *et al.* conducted a third set of *in vitro* experiments [141]. Similar to previous work, they hypothesized that THz radiation may elicit varied effects on the inhibition of DNA synthesis in synchronized versus asynchronized cells. They tested this hypothesis using both synchronous and asynchronous CHOPTK2 cells. The same evaluation techniques, FEL THz source, and exposure parameters were employed as described in Berns *et al.* [142] (Table 2). As shown in previous studies, the data shows that synchronous and asynchronous THz-exposed cells both exhibited significant DNA synthesis inhibition. Compared to the controls, the synchronous cells exhibited higher levels of inhibition than the asynchronous cells, 22% versus 17%, respectively. During these short exposures, the authors predicted that the temperature rise was 2.96°C (Fig. 7b).

Study 8. In a follow-up study to Kiselev's work [168], Makolinets *et al.* conducted an *in vitro* study to explore the effect that THz radiation has on the migration ability of both healthy and immunocompromised rat spleen cells [169]. Exposures were conducted using a FIR THz source using the following exposure parameters: exposure temperature (25°C), 0.89 THz, H=0.13–0.25 mWcm^{-2}, and 15 minute duration (Table 2). The authors evaluated the migration ability of the cells post-exposure, and the data indicates that the migration ability of the cells was enhanced by exposure to THz radiation. Although the authors do not report temperature measurements, our computational models predict that the rise in temperature is less than a 1°C during exposures.

Study 9. In 2002, Hadjiloucas *et al.* examined the effect that THz radiation has on the growth rate of yeast cells (*Saccharomyces cerevisiae*) [170]. Cells were exposed at room temperature (25°C) using a BWO THz source: 0.2–0.35 THz, 5.8 mWcm^{-2}, and exposure durations = 30, 60, 90, 120, or 150 min (Table 2). Microcolony growth areas were evaluated post-exposure using time-lapse photographic techniques, and temperatures were measured before, during, after exposure. The results of this work demonstrated that the cells exposed to THz radiation exhibited statistically significant increases in cell growth. For the 150 min exposure, the authors observed a 2–3°C temperature rise (Fig. 7b). Interestingly, mammalian cells exposed to temperatures of 27–28°C for greater than 100 min typically undergo "cold shock", affecting cell growth [166]. However, since yeast cells were used in this work, it is not clear what the impact of the cold shock would be on them. Therefore, the observed effects on growth rate may be contributed to both the THz exposure and the stress induced by the cold shock.

Study 10. In 2003, in one of the initial studies of the THz-Bridge project, Clothier and Bourne *et al.* investigated the effect that THz radiation has on human keratinocytes [19]. Keratinocytes were isolated from human skin samples, plated in polystyrene culture plates, and exposed at a temperature of 22°C using a Ti-Sapphire laser and optical excitation methods. Exposure parameters were the following: 0.1–2.7 THz, power = 1 mW, beam spot 0.1 cm^2, H=10 mWcm^{-2}, and exposure durations = 10, 20, 30 min (Table 2). Three samples were used for each exposure condition. Cellular viability was examined post-exposure using conventional assays. Data was analyzed using several statistical analysis techniques, including repeat measurement ANOVA and Dunnetts post hoc test. The authors report that THz-exposed cells did exhibit subtle increases in resazurin reduction, but these effects were not statistically significant when compared to control cells. The authors conclude that "normal keratinocytes do not appear to be adversely affected by THz radiation."

Study 11. In 2007, Federov *et al.* published a scientific proceeding that detailed the cellular effects observed in several cell lines exposed to THz radiation [171]. In this work, human red blood cells and lymphocytes were exposed to THz radiation provided by a FIR

THz laser source (NH_3 media and N_2O optical pump). The following exposure parameters were used: exposure temperature (25°C), 3.68 THz, 20 mW/cm^2, exposure durations of 30–90 min (Table 2). Several markers were evaluated post-exposure, including cell death, cell proliferation, and lipid membrane permeability. The data from this work demonstrated that THz-exposed red blood cells exhibited increases in both cellular proliferation and membrane permeability. Additionally, the THz-exposed lymphocytes exhibited increases in cellular proliferation and 38% of the exposed cell population died post-exposure. The authors did not measure the temperature rise during exposures, but our models indicate that the rise is less than or equal to 1.5°C (Fig. 7b).

Study 12. In 2008, Clothier and Bourne *et al.* conducted a follow up investigation to their 2003 study [172]. In this study, they investigated the effect that THz radiation has on several human cells lines: human epithelial keratinocytes, corneal, and ND7/23 cells. The cells were exposed at 22°C using a pulsed THz source with the following exposure parameters: 0.14–0.15 THz, 80 ns pulse duration, 24–62 mWcm^{-2}, and exposure durations from 10 to 1440 min (Table 2). Cellular viability, differentiation, membrane barrier permeability, heat shock protein, and glutathione (GSH) expression were examined post-exposure using conventional assays. The authors report that all THz-exposed cells did not exhibit detectable alterations.

Study 13. In 2008, Olshevskaya *et al.* examined the direct effects that THz radiation have on isolated neurons from *Lymnaea stagnalis* [20]. Exposures were conducted with a THz FEL using the following exposure parameters: frequencies of 0.7, 2.49, and 3.69 THz; H=0.3–30 mWcm^2, exposures ≥1 min (Table 2). The following effects were examined post-exposure: cell growth, neural network regeneration, cell adhesion, cell morphology, intracellular structural damage, and ability to maintain membrane potential. For all frequencies tested, the authors observed that THz radiation impacted cells in a dose-dependent manner, where subtle effects appeared at lower irradiances (≤1.0 mWcm^{-2}), and pronounced effects at higher irradiances (≥30 mWcm^{-2}) Specifically, the most significant effects were to cellular growth, adhesion (70–80% of exposed population), membrane morphology, intracellular structures, and neural resting membrane potential. Although temperatures were not measured in this study, our computational models predict that during exposures the temperature of the nerves increased by 2.0°C. Given the short duration of these exposures, significant thermal effects typically do not result from such conditions (Fig. 7b); therefore, the mechanism responsible for the observed effects remains unclear.

Study 14. Over the past few years, the Air Force Research Laboratory (AFRL) has conducted several experiments to examine the biological effects of THz radiation [119–122, 147]. The primary goal for these studies was to examine the cellular response of human mammalian cells exposed to high-power THz radiation using an optically-pumped molecular gas THz laser. In their first *in vitro* study, they exposed human dermal fibroblasts in a temperature-controlled chamber to THz radiation (2.52 THz, 84.8 mWcm^{-2}, durations: 5, 10, 20, 40, or 80 min) (Table 2) [119, 147]. To evaluate the temperature rise during their THz exposures they employed computational and empirical dosimetric techniques: FDTD modeling approaches, infrared cameras, and thermocouples. Cellular viability was assessed using conventional viability assays. The transcriptional activation of heat shock proteins and DNA sensing genes was evaluated using conventional qPCR techniques. In order to compare the THz-induced cellular responses, they also conducted comparable analyses for hyperthermic positive controls (39.8°C for 80 min) with matched thermal histories.

Data from this work shows that the computational and empirical dosimetric data were in agreement, and that the temperature of the cells increased by 2.9°C during each exposure. The viability data indicate that the percent of cell death increased with exposure duration, and was maximal for the 80 min exposure (5% cell death). Interestingly, the percent of cell

death and fold-increase of the heat shock proteins were comparable for both the THz and hyperthermic positive controls. In addition, the data showed that none of the DNA repair genes were up-regulated in the THz-exposed samples. The authors conclude that the results of this work suggest that the biological effects generated by THz radiation appear to be primarily photothermal in nature.

Study 15. Building on their preliminary investigation [119, 147], this group conducted a follow-up study to further examine the cellular response to THz radiation [120]. Specifically, several improvements were made to their previous approach: (i) computational and empirical dosimetric methods were refined; (ii) to increase statistical power of results: increased the number of samples exposed to both THz radiation and to hyperthermic stress; (iii) increased number of qPCR experiments to examine the gene expression of primary heat shock proteins and DNA repair sensing genes; (iv) conducted comparable analyses for well-established genotoxic controls (UV radiation) to closely examine effects of THz on DNA; and (v) evaluated and compared genetic response of cells exposed to THz, hyperthermic, and genotoxic stress. Aside from these differences, this work was conducted using the same cell line, THz source, dosimetric techniques, cellular response evaluation methods, and exposure parameters as described in Wilmink *et al.* [119, 147]. The results of this work indicate that cellular temperatures increased by 2.9–3.0°C during all THz exposures. In addition, for each exposure duration tested, the THz and hyperthermic exposure groups exhibited equivalent levels of cell death (≥10%) and 4-fold increases in heat shock protein expression. The qPCR data showed that the expression of cyclin E (CCNE2), a signature DNA sensing and repair gene, was unchanged in both the THz and heat shock exposure groups; however, appreciable increases (40-fold) were observed in the genotoxic controls (UV radiation). The authors conclude that dermal fibroblasts exhibited comparable cellular and molecular effects when exposed to THz radiation and hyperthermic stress, and that the effects observed are primarily thermal in nature.

Study 16. In a third THz bioeffects study [121], this group sought to answer two fundamental questions. First, do cells exposed to high-power THz radiation die via necrotic or apoptotic mechanisms? Second, do human cells express a signature gene expression profile when exposed to THz radiation? In this study, death thresholds and gene expression profiles were evaluated for several human cell lines exposed to high-power THz radiation (2.52 THz, 227 $mWcm^{-2}$, exposure durations: 5–40 min). Necrotic and apoptotic death thresholds were determined for Jurkat suspension cells using MTT viability assays and flow cytometric techniques. In addition, confocal microscopic techniques were used to demarcate lethal spatial regions in a monolayer of dermal fibroblasts exposed to THz radiation. To determine if cells exhibit a THz-specific gene expression signature, we exposed dermal fibroblasts to THz radiation and analyzed their transcriptional response using a state-of-the-art microarray gene chip: GeneChip® Human Genome U133 Plus 2.0 Array (Asuragen Inc, Austin, TX). This array offers comprehensive coverage of the expression level of over 47,000 transcripts and variants, including 38,500 well-characterized human genes.

The MTT viability data showed that 82% of the Jurkat cells died from the 40 min THz exposure, while the flow cytometry data showed that only 62% of the cells died from the exposure. The flow data also indicated that 32% of the dying cells exhibited early signs of apoptosis and 30% showed signs of necrosis. This data provided evidence that THz-induced cell death was mediated using both necrotic and apoptotic processes. The confocal microscopy data demonstrated that THz-exposed cells exhibited increased lipid membrane permeability. Last, the microarray data showed that dermal fibroblasts activated many of the fundamental cellular stress response pathways when exposed to THz radiation. In addition, the data indicated that several unique genes (i.e. cytokines, interleukins, apoptosis), which

were not expressed in hyperthermic controls, exhibited pronounced expression in THz-exposed cells. Overall, this work indicates that THz-induced cell death is mediated via both apoptotic and necrotic pathways. In addition, several genes appear to be preferentially expressed by cells exposed to THz radiation. This group also speculates that the identified up-regulated genes may serve as candidate biomarkers for THz exposures.

Study 17. In a recent study, Bock *et al.* examined the effect that THz radiation has on cellular gene expression [106]. In this study, microarray gene chip and PCR analyses were performed on mouse stem cells exposed to broadband THz radiation generated with frequency mixing techniques. Exposure conditions were the following: broadband THz radiation (centered at 10 THz), 1 $mWcm^{-2}$, repetition rate of 1 kHz, pulse duration 35 fs, 1 μJ/pulse, and exposure durations: 120, 240, 360, and 540 min). Temperature of the cells was measured before, during, and after exposures. Three independent measurements were performed and each was conducted in duplicate. All exposures were conducted at an ambient temperature of 26.3°C.

The authors report that no morphological effects were observed in all THz-exposed cells. However, they do indicate that "lipid droplet-like inclusions" did appear in the cytoplasm after 6 h of THz irradiation. Such effects were not observed in the shorter exposures, and the authors conclude that their appearance is dose dependent. Using IR cameras, the authors report a 0.3°C temperature rise in exposed cells. The authors report that the microarray data indicates that stem cells exhibit differential gene expression when exposed to THz radiation. The data shows roughly 6% of the differentially expressed genes increase in expression, 5% decrease, and 89% remain unchanged. The RT-PCR data confirmed that several genes were increased by up to 14-fold post-exposure: Adiponectin, GLUT4, FABP4, and PPARg. Additional experiments further confirmed that these changes in gene expression were time-dependent and were maximal for the 540 min exposure. Overall, this study provides evidence that cells exposed to THz radiation appear to differentially express several genes. Since the temperature rise is marginal during all exposures, it appears that other mechanisms may be responsible for the observed effects. The authors speculate that the observed effects may be in part due to the direct activation of transcription factors, and in particular for the promoter of peroxisome proliferator-activated receptor gamma (PPARG).

Study 18. Earlier this year, Federov *et al.* conducted a study [173] to examine the response of hamster fibroblasts exposed to THz radiation generated from a FIR source, as described in Federov *et al.* [171, 174]. Cells were exposed at a frequency of 3.68 THz, power of 20 mW, and exposure duration of 30, 60 or 90 minutes. Cellular activity was evaluated using conventional viability assays to measure the optical density of formazan crystals in mitochondria. The data indicates that cells exposed to THz radiation exhibited no significant signs of damage or cellular activity.

6.4 *In vitro* studies on lipid membranes

Study 1. In 2007, Ramundo-Orlando *et al.* conducted a series of experiments to explore the effect that pulsed THz radiation has on lipid membranes [18]. The authors hypothesized that THz radiation may cause rearrangement of the lipid bilayer that may lead to increases in membrane permeability. They tested this hypothesis using two types of enzyme-containing cationic liposomes: dipalymitoyl phoshatidylchonie (DPCC) and palmitoylo-leoyl phosphatidylchonine (POPC). Both liposomal models were loaded with carbonic anhydrase (CA) and the substrate p-nitrophenyl acetate (p-NPA) was added to the bulk aqueous phase. When liposomes were exposed to THz radiation, the trapped CA converts the p-NPA molecules into product with a peak absorbance at 400 nm, which was assessed using a spectrometer. The authors examined these effects using two THz sources: (1) compact FEL (cFEL) operating in pulsed mode: 0.13 THz, repetition rates of 5, 7, or 10 Hz,

50 ps pulse duration, 5–17 mWcm^{-2}, exposure duration 2 min; (2) IMPATT THz source operating in CW: 0.15 THz, 6.2 mWcm^{-2}, and exposure durations of 2 to 3 min (Table 2).

Results of this study indicate that liposomes exposed to CW irradiation did not exhibit increases in membrane permeability, but both liposomal models showed 2-fold increases in permeability when exposed to pulsed THz radiation (7–10 Hz and ≥7.7 mWcm^{-2}). Curiously, the observed effects were maximal at 7-Hz (Fig. 8a). The authors believe these effects may result from resonance-like mechanisms. They observed similar effects in a previous study where they used 7 Hz magnetic fields and the same liposomal model [175]. In this study, the authors reported small increases in temperature (0.05°C) during all exposures (Fig. 7b). Dressler *et al.* demonstrated that thermal stress protocols (51°C for 2 min) can cause significant effects to plasma membrane; however, they did not observe these effects at lower temperatures [70]. Assuming liposomal membranes have comparable thermosensitivities as cellular plasma membranes, the results of this work indicate that the membrane effect

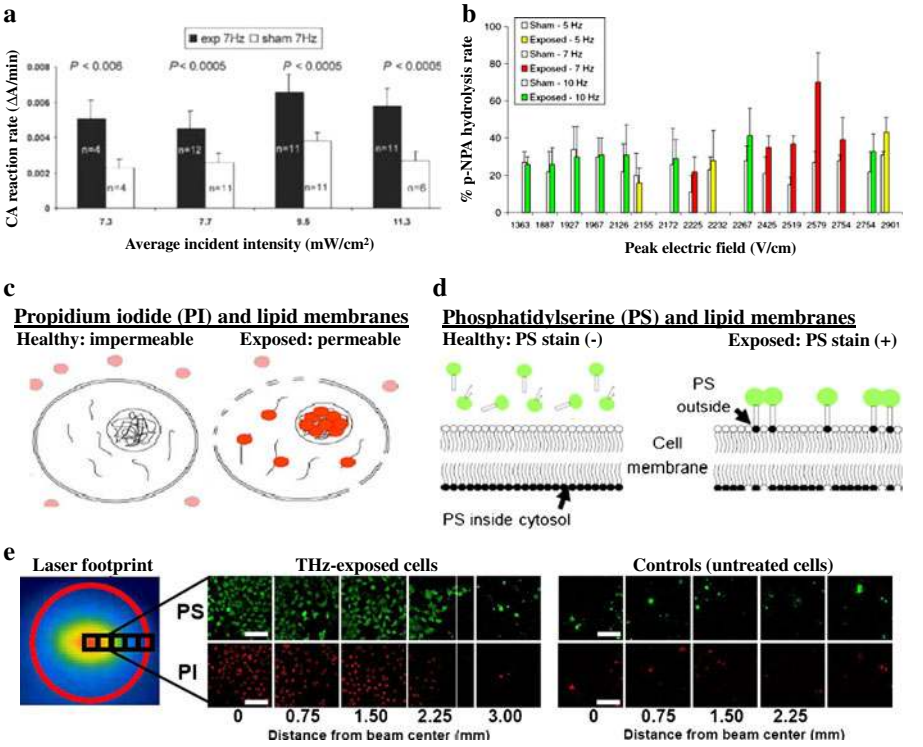

Fig. 8 (**a**–**e**) THz interactions with lipid membranes. **a**. Effects of pulsed THz radiation on liposome permeability. Increases in permeability are observed for irradiances greater than 7.3 mW/cm^{-2}. (Reprinted with permission from [18]. ©2007, Wiley-Liss, Inc.). **b**. Effects of pulsed 0.13 THz radiation on liposome permeability. Permeability increases as a function of peak electric field. (Reprinted with permission from [176]. ©2009, Springer Science). **c**. Propidium Iodide (PI) staining for detection of permeable membranes, typically exhibited by THz-exposed cells. PI is a fluorescent molecule (λ_{exc}=488 nm and λ_{em}=562–588 nm) that is impermeable to viable intact membranes but is permeable to cells with damaged membranes. **d**. Phosphatidylserine (PS): FITC-AV staining. Viable cells retain PS on the inner leaflet, but cells undergoing membrane reorganization externalize PS. FITC has excitation and emission spectrum peak wavelengths of 495 nm and 521 nm, respectively. **e**. Infrared microthermography and fluorescent images of dermal fibroblasts exposed to Terahertz Radiation and control cells (Left to Right) (20X objective, bar=100 μm). (Reprinted with permission from [119]. ©2010.

observed could be considered "nonthermal" and are "not simply caused by heating." Overall, this is a well-designed study, the authors used a sufficient sample size (n=5–16), tested multiple THz sources using various repetition rates, employed appropriate experimental controls, conducted empirical dosimetry, and conducted sufficient statistical analyses.

Study 2. In 2009, Ramundo-Orlando *et al.* conducted a follow-up study [176]. The goal for this study was to examine the effects of THz radiation as a function of electric field. Using similar approaches described in Ramundo-Orlando *et al.* [18], they examined the rate of p-PNA hydrolysis as a function of high electric field (1.0–3.0 $kVcm^{-1}$) (Table 2). It is interesting to note that these are high field strengths, which are roughly 10% of the field required to achieve air-breakdown (~30 $kVcm^{-1}$). Using the relationship I ($mWcm^{-2}$)=($cn\varepsilon_o/2)\times E^2$ where $c=2.99\times10^{10}$ $cm\times s^{-1}$, $n=3$, $\varepsilon_o=8.854\times10^{-9}$ $mW\times s\times cm^{-1}V^{-2}$, and E=1–3 $kVcm^{-1}$, these electric fields correspond to irradiances ranging between 4×10^6 and 3.6×10^7 $mWcm^{-2}$. Data from this work indicates that the permeability of liposomes increases as a function of electric field. These effects were maximal between 2.6–2.7 $kVcm^{-1}$ (Fig. 8b). The authors believe the observed effects may result from the "rectification of THz pulses by liposomes." The temperature rise during these exposures is assumed to be comparable to that observed in their previous study (~0.05°C) (Fig. 7b). Overall, this is a well-designed study, but several specific experimental details were omitted (i.e., sample population size, statistical approach, and beam diameter). These details would be helpful for more accurate dosimetry, and in particular for determining the THz irradiance incident on the membrane.

Study 3. In 2010, Wilmink *et al.* conducted a series of experiments to explore the effects that THz radiation have on the lipid membrane [121]. The primary goal for these studies was to use infrared microthermographic techniques and fluorescence imaging methods to explore the effect that THz radiation has on the cellular membrane permeability. To examine these effects, dermal fibroblasts were plated in 35-mm glass-bottom dishes and treated with THz radiation (2.52 THz, 227 $mWcm^{-2}$, and exposure duration of 0.2 min). Cells were stained with propidium (PI) and FITC-AV-PS (Annexin V-phosphatidyleserine), and imaged using a confocal laser scanning microscope (Zeiss LSM 710) In brief, PI is impermeable to healthy cells, but is permeable to exposed or porated cells. In contrast, in healthy cells PS resides on the inner leaflet of the membrane, while in stressed cells, PS is externalized and readily binds to FITC-AV (see Fig. 8c, d). Microthermographic infrared images were also collected for the THz-exposed cells.

The data shows that THz irradiation increased the temperature of the cells by 6°C (Fig. 8e). Fluorescent images were collected at 5 spatial regions, from the center to the periphery of the laser beam footprint. Cells positioned at the center of the THz beam footprint stained positive for both PI and PS, whereas cells at the periphery stained negative for both PI and PS. In addition, few control cells stained positive for both PI and PS (Fig. 8e). Fluorescence microscopy data showed that cells exposed to THz radiation for 12 seconds or less stained negative for both PI and FITC-AV; whereas exposures greater than 12 seconds stained positive for both PI and FITC-AV. The results of this work suggest high-power THz radiation may cause direct effects to the plasma membrane of human cells.

6.5 *In vitro* studies on biological macromolecules

6.5.1 DNA damage assessment / genetic toxicology

To the best of our knowledge, there are only 4 studies published in the literature where investigators have examined the extent of DNA damage in cells exposed to THz radiation.

Study 1. In 2003, Scarfi *et al.* conducted a study associated with the THz-Bridgeprogram [17] to investigate the effect of THz radiation on blood samples. In this study, peripheral

blood samples were collected from 9 healthy human volunteers. Samples were exposed to 0.12 or 0.13 THz generated from a FEL source using following operating conditions: pulsed wave, 50 pulses, 4 μs duration, 330 pulses interval, 1 or 0.6 mW power, 1.2 or 0.72 J energy [17]. Exposures were conducted at room temperature for 20 min. Aliquots of untreated blood samples were used as controls. The results showed that the number of micronuclei (MN) in THz-exposed and sham-exposed control cells was comparable. In addition, THz exposure did not affect the kinetics of lymphocyte proliferation. The authors conclude that the results of this report suggest that THz radiation does not cause chromosomal damage to lymphocytes. They also conclude that due to their small sample size, their results do not provide definitive conclusions, and they recommend that similar studies be performed using a larger sample size.

Study 2. In 2007, Zeni *et al.* conducted a study within the framework of the THz-Bridgeprogram to examine the genotoxic effects of THz radiation [16]. For this study, they obtained human blood lymphocytes from healthy human volunteers (n=17). Samples were irradiated at room temperature (23°C) using a compact FEL laser source with the following conditions: 0.12 or 0.13 THz, 4 μs pulse duration, repetition rate of 1–10 Hz, average power of 0.6–5.0 mW, irradiance of 0.05–0.23 $mWcm^{-2}$, peak electric fields 130–193 V cm^{-1}, and specific absorption rates of 0.24–2 W kg^{-1} [16]. Primary DNA damage (single strand breaks, SSB) was assessed using alkaline comet assays, and the incidence of MN was determined using conventional cytochalasin-block techniques. Using first principles, the authors predict that the temperature rise in the cells was roughly 0.35°C. The authors report that differences between the THz and control samples were not statistically significant. In addition, the cell cycle kinetics of the proliferating lymphocytes were not affected by the THz exposure.

Study 3. In 2008, Korenstein-Ilan *et al.* conducted a THz genotoxicity study in conjunction with the THz-Bridgeprogram [15]. In this work, human blood lymphocytes were exposed in an incubator (37±0.03°C) to CW THz radiation using an electronic, frequency up-conversion THz source. The following exposure parameters were used: 0.1 THz, 0.031 $mWcm^{-2}$, and exposure durations ranging from 60, 120, and 1440 min. The authors employed both empirical and computational dosimetric techniques to measure the THz-induced temperature rise during exposure. Fluorescence in situ hybridization (FISH) techniques were used to determine the incidence of aneuploidy with centromere-specific probes for chromosomes 1, 10, 11, and 17.

The results were the following: (i) chromosomes 11 and 17 were most vulnerable (about 30% increase in aneuploidy after 2 and 24 h of exposure); (ii) chromosomes 1 and 10 were not affected; (iii) asynchronous mode of replication of centromeres was increased by 40% in chromosomes 11, 17 and 1 after 2 h of exposure, and was increased by 50% in all four centromeres after 24 h of exposure. The authors report that "our results demonstrate that exposure of lymphocytes *in vitro* to a low power density of 0.1 THz radiation induces genomic instability. These findings, if verified, may suggest that such exposure may result in an increased risk of cancer." These observations and statements must be viewed with caution. The authors have stimulated the lymphocytes with PHA for 1–6 hours before exposures to THz for 1, 2 and 24 hours. During this period (1–6 hours before THz exposure +1, 2 and 24 hours of THz exposure) the cells will still be in G0-G1-S-phase stage of the cell cycle, assuming the G1-phase takes 6–8 hours and the S-phase takes 24–30 hours [177, 178]. The G2-phase of the cell cycle typically begins 45 h after initial culture, and during cell division/mitosis the spindle acts to segregate the chromosomes equally into 2 daughter cells. It is well known that aneuploid cells can arise as a consequence of disturbances in spindle action(s) leading to unequal distribution of chromosomes into daughter cells. Per the experimental protocol used by the authors, THz exposures might not have acted directly on mitotic spindles to induce aneuploidy when PHA-stimulated lymphocytes (1–6 hours) were exposed for 1, 2 and 24 hours. Moreover, the

incidence of MN, which are caused by spindle disturbances as well as from broken chromosomes, are reported to occur in roughly 9.0±8.0 in 8,667 samples [179]. Assuming that all aneuploid cells recorded by the authors eventually appeared as micronucleated lymphocytes, the overall incidence of aneuploidy of all chromosomes (1, 10, 11 and 17) in 24 hour THz-exposed and sham-exposed control cells reported by the authors was 10.6±5.5% and 9.0±5.2%, respectively. These indices are within the spontaneous levels reported in the historical data base [179]; thus, this data may be interpreted as an absence of significantly increased aneuploid cells following exposure to THz.

Study 4. Earlier this year, Federov *et al.* conducted an *in vitro* study to investigate the effects that THz radiation has on lypholized DNA [173]. In this work, the authors used the THz source described in [170], with the following exposure conditions: 3.68 THz, 20 $mWcm^{-2}$, and exposure durations of 10, 30, or 60 min. Exposures were conducted at room temperature for 20 minutes. To examine conformational changes in DNA, the authors used UV spectroscopy. The data shows that THz radiation caused changes in the optical density of the nucleotides at UV wavelengths. These effects were observed to be dose-dependent and the spectral changes were most pronounced at wavelengths between 190–220 nm and 240–280 nm. These results provide evidence that THz radiation may cause conformational or structural changes to DNA.

6.5.2 Enzyme activity

Study 1. In 1991, Govurun *et al.* performed a set of experiments to examine the effect that THz radiation has on several biomolecules, including albumin, alcohol dehydrogenase, peroxidase, and trypsin [180]. The authors exposed biomolecules to irradiation using a FIR THz source with the following operating conditions: 3.33 THz, 5 mJ per pulse, 40–600 pulses, and a total energy of 0.2 to 3 J. Rate reaction measurements were conducted using a UV spectrophotometer, and protein structure was assessed using a circular dichroism spectropolarimeter (290 nm). The data shows that enzyme activity was dependent on the dose of THz irradiation. The authors report that structural changes (i.e., alpha helices and random coils) were observed in albumin exposed to THz radiation. The authors conclude that this data suggests that THz radiation can exert structural changes in proteins.

Study 2. In 2009, Homenko *et al.* examined the direct effects of THz radiation on two enzymatic processes: (i) the interaction of soluble or immobilized alkaline phosphatase (AP) with the substrate p-nitrophenylphosphate; and (ii) the interaction between an antibody and its antigen [14]. Both enzymatic processes were exposed to THz radiation generated using an electronic, frequency multiplier THz source. The following exposure conditions were employed: 0.1 THz, 0.08 $mWcm^{-2}$, and exposure durations of 60–120 min. The data shows that the effects of THz radiation on soluble AP are not statistically significant. Immobilization of the enzyme also appeared to make AP less prone to the effects caused by the THz exposures. In contrast, the authors reported that THz radiation did, in fact, cause statistically significant decreases in the interaction of the antibody-antigen complex. The authors conclude that "exposure to low level THz radiation may interfere with the interaction of protein recognition molecules, such as enzymes and anitbodies with small molecular substrates."

6.5.3 Albumin

Study 1. In 2009, Cherkasova *et al.* examined the direct effects of THz radiation on spectral and functional properties of albumin [22]. In this work, the authors exposed lypholized bovine serum albumin (BSA) to THz radiation using a FIR THz source (3.6 THz, 10

$mWcm^{-2}$, 60 min). The effects on BSA spectra were evaluated using UV absorption spectrophotometer and a circular dichroism (CD) spectropolarimeter. Spectra were recorded repeatedly 30, 60, 120, and 150 min post-exposure. The data shows that THz radiation causes statistically significant changes to the UV and CD spectra of albumin. These effects are dose-dependent, and the authors contend that these effects suggest that the spectral changes are indicative of conformational changes in the protein molecule resulting from exposure to THz radiation.

Study 2. In 2009, Federov *et al.* examined the direct effects of THz radiation on spectral and functional properties of BSA [181]. The authors irradiated BSA using a Ti:Sapphire based THz source using the following exposures conditions: 0.05–1.3 THz, 150 nW, pulsed power 750 μW, a 2.5 ps pulse duration, exposure duration of 30 min. The effects on BSA spectra were evaluated using a UV absorption spectrophotometer. The data reported indicates that THz radiation causes statistically significant changes to the UV spectra of albumin, and that these effects are most pronounced in the 240–290 nm range. The authors conclude that these effects are a result of preferential absorption of the hydration shell surrounding the BSA molecules.

6.5.4 Hemoglobin

Study 1. In 1991, Ilyina *et al.* examined the effects that THz radiation has on hemoglobin (Hb) bonds [136]. In this work, the authors irradiated Hb bonds to THz radiation provided by a BWO source: 2.65 THz and 3.33 THz, 3 $mWcm^{-2}$, and exposure duration of 240 min. Interestingly, the data shows that THz radiation caused an increase in Hb bond strength at 3.33 THz, and a decrease in bond strength at 2.65 THz. The authors hypothesize that the observed effect is a result of linear or nonlinear resonance effects.

7 Summary & future prospects

Knowledge of the biological effects associated with THz radiation is critical for proper health hazard evaluation, development of empirically-based safety standards, and safe exploitation of new THz devices and applications. The studies reviewed in this report provide data on the effects of THz radiation at an organism, tissue, organelle, cellular, and biomolecular level. Each publication was critically analyzed and the effects observed have been summarized.

For the *in vivo* studies conducted on vertebrates (i.e., humans, rats, and mice), THz treatments stimulated wound repair, enhanced microbial dissemination, increased fibrinolysis factors, and reduced platelet aggregation. In contrast, for the *in vivo* studies using fruit flies, THz exposures induced differential expression of several proteins. In the studies using a plant model, exposures stimulated the growth of paddy rice, black beans, and wheat. In the *ex vivo* tissue studies, visible tissue damage was observed after exposures to short duration (2 seconds), high-power THz radiation (7.16 Wcm^{-2}).

In several *in vitro* cell culture studies, low doses of THz radiation stimulated cellular proliferation, whereas higher exposures caused visible morphological changes, induction of cellular stress response mechanisms, and cell death. THz radiation (both CW and pulsed) caused direct effects on the plasma membrane: increases in membrane permeability, membrane reorganization, and destruction. For the studies examining the effects on biomolecules, THz exposures were observed to affect both the structure and functional activity of several enzymatic processes. Finally, the majority of the genotoxicity studies performed to date show that THz radiation does not cause adverse effects to DNA structure or function.

In future studies, special care should be placed to address several key elements. In particular, sufficient details need to be provided regarding THz sources, detectors, exposure chambers, and dosimetric tools. Specifically, the following details are fundamental: (i) exposure duration and incident THz irradiance on biological sample; (ii) characterization of THz beam quality; (iii) detailed specifications of the detector (i.e., temperature of operation, aperture size, damage thresholds, sensitivity (NEP), and response time). (iv) use of gas- and temperature-controlled exposure chambers for *in vitro* exposures; and (v) use of empirical and computational modeling dosimetric analysis.

In addition to these fundamental considerations, emphasis should be placed to ensure that the experimental design and analysis is sufficient. Specifically, the following considerations should be addressed: (i) experimental design includes several experimental controls: negative controls (unexposed), sham exposured samples and positive controls (heat, UV radiation); (ii) the proper population size is selected using statistical power methods; (iii) all in vitro exposures should be conducted in temperature-controlled exposure chambers; and (iv) all experimental details regarding source, detector, and exposure conditions are provided, including type of THz source, frequency, operation type (CW or pulsed), repetition rate, pulse duration, exposure duration, irradiance, temperature of exposure chamber, and dosimetric data.

In summary, the use of the above practices should help reduce the number of confounding variables. These measures will hopefully help ensure that effects observed in future studies are fully attributable to the THz radiation. Such measures will also help provide researchers with more definitive evidence as to whether the observed effects are due to the macroscopic thermal effects associated with the exposures.

Acknowledgements We wish to thank the National Academy of Sciences NRC Research Associateship program and the Air Force Research Laboratory for providing the opportunity to conduct this study. In particular, we would like to thank Frank Ruhr for his dedication and attention to detail in design of the THz enclosure, and Dr. Morley Stone for his consistent support over the past few years. This work was supported by AFRL. In closing, the authors also wish to dedicate this invited review article to Dominic Cameratta, a man who always provided us with inspiration.

References

1. Thruvision. 2010 [cited 15 Nov. 2010]; Available from: http://www.thruvision.com/index.html.
2. Brijot. 2010 [cited 15 Nov. 2010]; Available from: http://www.brijot.com/contact-us/.
3. Taylor, Z.D., *et al.*, *Reflective terahertz imaging of porcine skin burns.* Opt. Lett., 2008. **33**(11): p. 1258–1260.
4. Ashworth, P.C., *et al.*, *Terahertz pulsed spectroscopy of freshly excised human breast cancer.* Opt Express, 2009. **17**(15): p. 12444–54.
5. Brun, M.-A. and *et al.*, *Terahertz imaging applied to cancer diagnosis.* Physics in Medicine and Biology, 2010. **55**(16): p. 4615.
6. Wallace, V.P., *et al.*, *Terahertz pulsed imaging and spectroscopy for biomedical and pharmaceutical applications.* Faraday Discuss, 2004. **126**: p. 255–63.
7. Woodward, R.M., *et al.*, *Terahertz pulse imaging in reflection geometry of human skin cancer and skin tissue.* Phys Med Biol, 2002. **47**(21): p. 3853–63.
8. Woodward, R.M., *et al.*, *Terahertz pulse imaging of ex vivo basal cell carcinoma.* J Invest Dermatol, 2003. **120**(1): p. 72–8.

9. Federici, J.F., *et al.*, *THz imaging and sensing for security applications: explosives, weapons and drugs.* Semiconductor Science and Technology, 2005. **20**(7): p. S266-S280.
10. Bogue, R., *Terahertz imaging: a report on progress.* Sensor Review, 2009. **29**(1): p. 6–12.
11. Dobroiu, A., C. Otani, and K. Kawase, *Terahertz-wave sources and imaging applications.* Measurement Science and Technology, 2006. **17**(11): p. R161-R174.
12. Smye, S.W., *et al.*, *The interaction between terahertz radiation and biological tissue.* Phys Med Biol, 2001. **46**(9): p. R101-12.
13. Walker, G.C., *Two Methods for Modelling the Propagation of Terahertz Radiation in a Layered Structure.* Journal of Biological Physics, 2003. **29**: p. 141–148.
14. Homenko, A., *et al.*, *Effects of 100 GHz radiation on alkaline phosphatase activity and antigen-antibody interaction.* Bioelectromagnetics, 2009. **30**(3): p. 167–175.
15. Korenstein-Ilan, A., *et al.*, *Terahertz radiation increases genomic instability in human lymphocytes.* Radiation Research, 2008. **170**(2): p. 224–234.
16. Zeni, O., *et al.*, *Cytogenetic observations in human peripheral blood leukocytes following in vitro exposure to THz radiation: a pilot study.* Health Phys, 2007. **92**(4): p. 349–57.
17. Scarfi, M.R., *et al.*, *THz Exposure of Whole Blood for the Study of Biological Effects on Human Lymphocytes.* Journal of Biological Physics, 2003. **29**(2): p. 171–176.
18. Ramundo-Orlando, A., *et al.*, *Permeability changes induced by 130 GHz pulsed radiation on cationic liposomes loaded with carbonic anhydrase.* Bioelectromagnetics, 2007. **28**(8): p. 587–598.
19. Clothier, R.H. and N. Bourne, *Effects of THz Exposure on Human Primary Keratinocyte Differentiation and Viability.* Journal of Biological Physics, 2003. **29**(2): p. 179–185.
20. Olshevskaya, J.S., *et al.*, *Effect of terahertz electromagnetic waves on neurons systems.* Computational Technologies in Electrical and Electronics Engineering, 2008. SIBIRCON 2008. IEEE Region 8 International Conference on, 2008: p. 210–211.
21. Fedorov, P. S.S, and P. A.N., *Dynamic Effects of Submillimeter Wave Radiation on Biological Objects of Various Levels of Organization.* International Journal of Infrared and Millimeter Waves, 2003. **24**(8): p. 1235–1254.
22. Cherkasova, O., *et al.*, *Influence of terahertz laser radiation on the spectral characteristics and functional properties of albumin.* Optics and Spectroscopy, 2009. **107**(4): p. 534–537.
23. Jacques, S.L. and D.J. McAuliffe, *The melanosome: threshold temperature for explosive vaporization and internal absorption coefficient during pulsed laser irradiation.* Photochem Photobiol, 1991. **53**(6): p. 769–75.
24. Tewari, P., *et al. Role of collagen in terahertz absorption in skin*. 2009: SPIE. **7169**: p. 71691A1–8.
25. Ruggeri, A. and P.M. Motta, *Ultrastructure of the connective tissue matrix*. Electron microscopy in biology and medicine. 1984, Boston: M. Nijhoff Publishers. 217 p.
26. Alberts, B., J.H. Wilson, and T. Hunt, *Molecular biology of the cell*. 5th ed. 2008, New York: Garland Science. xxxiii, 1601, 90 p.
27. Urano, M. and E. Douple, *Hyperthermia and Oncology: thermal effects on cells and tissues*. Hyperthermia and Oncology. Vol. 1. 1988, Utrecht, Netherlands: VSP BV.
28. Schulze, H., T. Kolter, and K. Sandhoff, *Principles of lysosomal membrane degradation: Cellular topology and biochemistry of lysosomal lipid degradation.* Biochimica et Biophysica Acta (BBA) - Molecular Cell Research, 2009. **1793**(4): p. 674–683.
29. Reddy, A., E.V. Caler, and N.W. Andrews, *Plasma Membrane Repair Is Mediated by Ca2+−Regulated Exocytosis of Lysosomes.* Cell, 2001. **106**(2): p. 157–169.
30. Ramzan, R., *et al.*, *Mitochondrial respiration and membrane potential are regulated by the allosteric ATP-inhibition of cytochrome c oxidase.* Biochim Biophys Acta, 2010. **1797**(9): p. 1672–80.
31. Blokhina, O., E. Virolainen, and K.V. Fagerstedt. *Antioxidants, oxidative damage and oxygen deprivation stress: a review.* Ann Bot, 2003. **91**(2): p. 179–94.
32. Kindt, J.T. and C.A. Schmuttenmaer, *Far-Infrared Dielectric Properties of Polar Liquids Probed by Femtosecond Terahertz Pulse Spectroscopy* The Journal of Physical Chemistry, 1996. **100**(24): p. 10373–10379.
33. Venables, D. and C. Schmuttenmaer, *Spectroscopy and dynamics of mixtures of water with acetone, acetonitrile, and methanol.* Journal of Chemical Physics, 2000. **113**(24): p. 11222–11236.
34. Venables, D.S., A. Chiu, and C.A. Schmuttenmaer, *Structure and dynamics of nonaqueous mixtures of dipolar liquids. I. Infrared and far-infrared spectroscopy.* The Journal of Chemical Physics, 2000. **113**(8): p. 3243–3248.
35. Venables, D.S. and C.A. Schmuttenmaer, *Far-infrared spectra and associated dynamics in acetonitrile–water mixtures measured with femtosecond THz pulse spectroscopy.* The Journal of Chemical Physics, 1998. **108**(12): p. 4935–4944.
36. Segelstein, D., *The Complex Refractive Index of Water*. 1981, University of Missouri: Kansas City, MO.
37. Thrane, L., *THz Reflection Spectroscopy of liquid water.* 1995. **240**(4): p. 4.
38. Jepsen, P.U. and B.M. Fischer, *Dynamic range in terahertz time-domain transmission and reflection spectroscopy.* Opt Lett, 2005. **30**(1): p. 29–31.

39. Jepsen, P.U., J.K. Jensen, and U. Moller, *Characterization of aqueous alcohol solutions in bottles with THz reflection spectroscopy.* Opt Express, 2008. **16**(13): p. 9318–31.
40. Jepsen, P.U. and S.R. Keiding, *Radiation patterns from lens-coupled terahertz antennas.* Opt Lett, 1995. **20**(8): p. 807–9.
41. Jepsen, P.U., U. Moller, and H. Merbold, *Investigation of aqueous alcohol and sugar solutions with reflection terahertz time-domain spectroscopy.* Opt Express, 2007. **15**(22): p. 14717–37.
42. Wilmink, G.J., B.L. Ibey, and W.P. Roach, *Development of a Compact Terahertz Time Domain Spectroscopy System for the Measurement of the Optical Properties of Skin.* Journal of Biomedical Optics, 2011. **16**(4): p. 047006-047006–10.
43. Wilmink, G.J. and W.P. Roach, *Measurement of the optical properties of skin using terahertz time-domain spectroscopic techniques.* BiOS Proceedings of SPIE, 2010. **7562**: p. 75620J-75620J–4.
44. Pal, S.K., J. Peon, and A.H. Zewail, *Ultrafast surface hydration dynamics and expression of protein functionality: alpha -Chymotrypsin.* Proc Natl Acad Sci U S A, 2002. **99**(24): p. 15297–302.
45. Pal, S.K., J. Peon, and A.H. Zewail, *Biological water at the protein surface: dynamical solvation probed directly with femtosecond resolution.* Proc Natl Acad Sci U S A, 2002. **99**(4): p. 1763–8.
46. Pal, S.K. and A.H. Zewail, *Dynamics of water in biological recognition.* Chem Rev, 2004. **104**(4): p. 2099–123.
47. Pal, S.K., *et al.*, *Site- and sequence-selective ultrafast hydration of DNA.* Proc Natl Acad Sci U S A, 2003. **100**(24): p. 13746–51.
48. Pal, S.K., L. Zhao, and A.H. Zewail, *Water at DNA surfaces: ultrafast dynamics in minor groove recognition.* Proc Natl Acad Sci U S A, 2003. **100**(14): p. 8113–8.
49. Ladanyi, B.M. and M.S. Skaf, *Computer Simulation of Hydrogen-Bonding Liquids.* Annual Review of Physical Chemistry, 1993. **44**(1): p. 335–368.
50. Russo, D., G. Hura, and T. Head-Gordon, *Hydration dynamics near a model protein surface.* Biophys J, 2004. **86**(3): p 1852–62.
51. Yada, H., M. Nagai, and K. Tanaka, *Origin of the fast relaxation component of water and heavy water revealed by terahertz time-domain attenuated total reflection spectroscopy.* Chemical Physics Letters, 2008. **464**(4–6): p. 166–170.
52. Walther, M., *et al.*, *Far-infrared vibrational spectra of all-trans, 9-cis and 13-cis retinal measured by THz time-domain spectroscopy.* Chemical Physics Letters, 2000. **332**(3–4): p. 389–395.
53. Globus, T., *THz-Spectroscopy of biological molecules.* Journal of Biological Physics, 2003. **29**(2): p. 89–100.
54. Xie, A., *Excited-State Lifetimes of Far-Infrared Collective Modes in Proteins.* Journal of Biological Physics, 2002. **28**: p. 147–154.
55. Fischer, B., *et al.*, *Terahertz time-domain spectroscopy and imaging of artificial RNA.* Opt Express, 2005. **13**(14): p. 5205–15.
56. Fischer, B.M., *Broadband THz Time-Domain Spectroscopy of Biomolecules*, in *Mathematics and Physics*. 2005, Albert-Ludwigs-Universitat: Freiburg im Bresigau. p. 246.
57. Tuchin, V., *Handbook of Photonics for Biomedical Science*. 1 ed. Series in Medical Physics and Biomedical Engineering ed. C.P.T.F. Group. Vol. 1. 2010, Boca Raton: CRC Press 868.
58. Welch, A.J. and M.J.C.v. Gemert, *Optical-thermal response of laser-irradiated tissue*. Lasers, photonics, and electro-optics. 1995, New York: Plenum Press. xxvi, 925 p.
59. Pennes, H.H., *Analysis of Tissue and Arterial Blood Temperatures in the Resting Human Forearm.* Journal of Applied Physiology, 1948. **1**(2): p. 93–122.
60. Wang, L.V. and H.-i. Wu, *Biomedical optics: principles and imaging*. 2007, Hoboken, N.J.: Wiley-Interscience. xiv, 362 p.
61. Moritz, A.R., *Studies of Thermal Injury: III. The Pathology and Pathogenesis of Cutaneous Burns. An Experimental Study.* Am J Pathol, 1947. **23**(6): p. 915–41.
62. Moritz, A.R. and F.C. Henriques, *Studies of Thermal Injury: II. The Relative Importance of Time and Surface Temperature in the Causation of Cutaneous Burns.* Am J Pathol, 1947. **23**(5): p. 695–720.
63. Henriques, F.C. and A.R. Moritz, *Studies of Thermal Injury: I. The Conduction of Heat to and through Skin and the Temperatures Attained Therein. A Theoretical and an Experimental Investigation.* Am J Pathol, 1947. **23**(4): p. 530–49.
64. Vogel, A. and V. Venugopalan, *Mechanisms of pulsed laser ablation of biological tissues.* Chem Rev, 2003. **103**(2): p. 577–644.
65. Berry, E., *et al.*, *Do in vivo terahertz imaging systems comply with safety guidelines?* Journal of Laser Applications, 2003. **15**(3): p. 192–198.
66. Wilmink, G.J., *et al.*, *Molecular imaging-assisted optimization of hsp70 expression during laser-induced thermal preconditioning for wound repair enhancement.* J Invest Dermatol, 2009. **129**(1): p. 205–16.
67. Wilmink, G.J., *et al.*, *Assessing laser-tissue damage with bioluminescent imaging.* Journal of Biomedical Optics, 2006. **11**(4): p. 041114.

68. Wilmink, G.J., *et al.*, *In-vivo optical imaging of hsp70 expression to assess collateral tissue damage associated with infrared laser ablation of skin.* Journal of Biomedical Optics, 2008. **13**(5): p. 054066.
69. Wilmink, G.J., *et al.*, *Identification of microRNAs associated with hyperthermia-induced cellular stress response.* Cell Stress Chaperones, 2010. **15**(6): p. 1027–38.
70. Dressler, C., *et al.*, *Microscopical heat stress investigations under application of quantum dots.* Journal of Biomedical Optics, 2005. **10**(4): p. 041209–9.
71. Beuthan, J., C. Dressler, and O. Minet, *Laser-induced fluorescence detection of quantum dots redistributed in thermally stressed tumor cells.* Laser Physics, 2004. **14**(2): p. 213–219.
72. de Gannes, F.M.-P., *et al.*, *Metabolic and cellular characterization of immortalized humanmicroglial cells under heat stress.* Neurochemistry International, 1998. **33**(1): p. 61–73.
73. Roti Roti, J.L., N. Uygur, and R. Higashikubo, *Nuclear protein following heat shock: protein removal kinetics and cell cycle rearrangements.* Radiat Res, 1986. **107**(2): p. 250–61.
74. Beckham, J.T., *et al.*, *Assessment of cellular response to thermal laser injury through bioluminescence imaging of heat shock protein 70.* Photochem Photobiol, 2004. **79**(1): p. 76–85.
75. Beckham, J.T., *et al.*, *Role of HSP70 in cellular thermotolerance.* Lasers Surg Med, 2008. **40**(10): p. 704–15.
76. Beckham, J.T., *et al.*, *Microarray analysis of cellular thermotolerance.* Lasers in Surgery and Medicine, 2010. **42**(10): p. 752–765.
77. Diller, K.R., *Stress protein expression kinetics.* Annu Rev Biomed Eng, 2006. **8**: p. 403–24.
78. Kultz, D., *Evolution of the cellular stress proteome: from monophyletic origin to ubiquitous function.* J Exp Biol, 2003. **206**(Pt 18): p. 3119–24.
79. Kultz, D., *Molecular and evolutionary basis of the cellular stress response.* Annu Rev Physiol, 2005. **67**: p. 225–57.
80. Harmon, B.V., *et al.*, *Cell death induced in a murine mastocytoma by 42–47 degrees C heating in vitro: evidence that the form of death changes from apoptosis to necrosis above a critical heat load.* Int J Radiat Biol, 1990. **58**(5): p. 845–58.
81. Nishiyama, H., *et al.*, *A Glycine-rich RNA-binding Protein Mediating Cold-inducible Suppression of Mammalian Cell Growth.* The Journal of Cell Biology, 1997. **137**(4): p. 899–908.
82. Kaneko, Y., *et al.*, *A Novel hsp110-related Gene, apg-1, That Is Abundantly Expressed in the Testis Responds to a Low Temperature Heat Shock Rather than the Traditional Elevated Temperatures.* Journal of Biological Chemistry, 1997. **272**(5): p. 2640–2645.
83. Fujita, J., *Cold shock response in mammalian cells.* J Mol Microbiol Biotechnol, 1999. **1**(2): p. 243–55.
84. Roti Roti, J.L., *Cellular responses to hyperthermia (40–46 degrees C): cell killing and molecular events.* Int J Hyperthermia, 2008. **24**(1): p. 3–15.
85. Lepock, J.R., *Involvement of membranes in cellular responses to hyperthermia.* Radiat Res, 1982. **92** (3): p. 433–8.
86. Dewey, W.C., *et al.*, *Cellular responses to combinations of hyperthermia and radiation.* Radiology, 1977. **123**(2): p. 463–74.
87. Macouillard-Poulletier de Gannes, F., *et al.*, *Mitochondrial impairment and recovery after heat shock treatment in a human microglial cell line.* Neurochemistry International, 2000. **36**(3): p. 233–241.
88. Konings, A.W.T. and A.C.C. Ruifrok, *Role of Membrane Lipids and Membrane Fluidity in Thermosensitivity and Thermotolerance of Mammalian Cells.* Radiation Research, 1985. **102**(1): p. 86–98.
89. Guffy, M.M., *et al.*, *Effect of Cellular Fatty Acid Alteration on Hyperthermic Sensitivity in Cultured L1210 Murine Leukemia Cells.* Cancer Research, 1982. **42**(9): p. 3625–3630.
90. Dressler, C., *et al.*, *Fluorescence imaging of heat-stress induced mitochondrial long-term depolarization in breast cancer cells.* J Fluoresc, 2006. **16**(5): p. 689–95.
91. Nijhuis, E.H., *et al.*, *Induction of apoptosis by heat and gamma-radiation in a human lymphoid cell line; role of mitochondrial changes and caspase activation.* Int J Hyperthermia, 2006. **22**(8): p. 687–98.
92. Doulias, P.T., *et al.*, *Involvement of heat shock protein-70 in the mechanism of hydrogen peroxide-induced DNA damage: the role of lysosomes and iron.* Free Radic Biol Med, 2007. **42**(4): p. 567–77.
93. Turano, C., *et al.*, *The biochemical mechanism of selective heat sensitivity of cancer cells. 3. Studies on lysosomes.* Eur J Cancer, 1970. **6**(2): p. 67–72.
94. Harris, J.W., *Factors influencing the apparent radiosensitivity and heat stability of isolated leucocyte lysosomes.* Int J Radiat Biol Relat Stud Phys Chem Med, 1966. **11**(5): p. 465–76.
95. Hume, S.P., M.A. Rogers, and S.B. Field, *Heat-induced thermal resistance and its relationship to lysosomal response.* Int J Radiat Biol Relat Stud Phys Chem Med, 1978. **34**(6): p. 503–11.
96. Roti Roti, J.L., *Heat-induced alterations of nuclear protein associations and their effects on DNA repair and replication.* Int J Hyperthermia, 2007. **23**(1): p. 3–15.
97. Warters, R.L., *et al.*, *Heat shock (45 degrees C) results in an increase of nuclear matrix protein mass in HeLa cells.* Int J Radiat Biol Relat Stud Phys Chem Med, 1986. **50**(2): p. 253–68.

98. Higashikubo, R., N. Uygur, and J.L. Roti Roti, *Role of RNA and protein synthesis and turnover in the heat-induced increase in nuclear protein.* Radiat Res, 1986. **106**(2): p. 278–82.
99. Frohlich, H., *The extraordinary dielectric properties of biological materials and the action of enzymes.* Proc Natl Acad Sci U S A, 1975. **72**(11): p. 4211–5.
100. Frohlich, H., *Further evidence for coherent excitations in biological systems.* Phys Letters, 1985. **110A** (9): p. 80–81.
101. Alexandrov, B.S., *et al.*, *DNA breathing dynamics in the presence of a terahertz field.* Physics Letters A, 2010. **374**(10): p. 1214–1217.
102. Chitanvis, S.M., *Can low-power electromagnetic radiation disrupt hydrogen bonds in dsDNA?* Journal of Polymer Science Part B: Polymer Physics, 2006. **44**(18): p. 2740–2747.
103. Reimers, J.R., *et al.*, *Weak, strong, and coherent regimes of Fröhlich condensation and their applications to terahertz medicine and quantum consciousness.* Proceedings of the National Academy of Sciences, 2009. **106**(11): p. 4219–4224.
104. Alexandrov, B.S., *Pre-melting dynamics of DNA and its relation to specific functions.* Journal of Physics: Condensed Matter, 2009. **21**(3): p. 034107.
105. Swanson, E., *Modelling DNA Response to THz Radiation.* Phys. Rev. E., 2010.
106. Bock, J., *et al.*, *Mammalian stem cells reporgramming in response to Terahertz Radiation* PLoS Biol, 2010. **5**(12): p. e15806.
107. Ferguson, B. and X.-C. Zhang, *Materials for terahertz science and technology.* 2002. **1**(1): p. 26–33.
108. Hosako, I., *et al.*, *At the dawn of a new era in terahertz technology.* Proceedings of the IEEE, 2007. **95** (8): p. 1611–1623.
109. Lee, M. and M.C. Wanke, *Applied physics. Searching for a solid-state terahertz technology.* Science, 2007. **316**(5821): p. 64–5.
110. Liu, H.-B., *et al.*, *Terahertz spectroscopy and imaging for defense and security applications.* Proceedings of the IEEE, 2007. **95**(8): p. 1514–1527.
111. Siegel, P.H., *Terahertz technology.* Microwave Theory and Techniques, IEEE Transactions on, 2002. **50** (3): p. 910–928.
112. Sirtori, C., *Quantum cascade lasers: breaking energy bands.* 2009. **3**(1): p. 13–15.
113. Tonouchi, M., *Cutting-edge terahertz technology.* Nature Photonics, 2007. **1**(2): p. 97–105.
114. Williams, B.S., *Terahertz quantum-cascade lasers.* Nature Photonics, 2007. **1**(9): p. 517–525.
115. Wolbarst, A.B. and W.R. Hendee, *Evolving and experimental technologies in medical imaging.* Radiology, 2006. **238**(1): p. 16–39.
116. Lee, Y.-S., *Principles of Terahertz Science and Technology*, ed. Springer. 2009, Berlin: Springer
117. Crocker, A., *et al.*, *Stimulated Emission in the Far Infra-Red.* Nature, 1964. **201**(4916): p. 250–251.
118. Dodel, G., *On the history of far-infrared (FIR) gas lasers: Thirty-five years of research and application.* Infrared Physics & Technology, 1999. **40**(3): p. 127–139.
119. Wilmink, G.J., *et al. Quantitative investigation of the bioeffects associated with terahertz radiation*. in *Optical Interactions with Tissues and Cells XXI*. 2010: SPIE. **7562**: pp. 75620L-75620L-10.
120. Wilmink, G.J., *et al.*, *In vitro investigation of the biological effects associated with human dermal fibroblasts exposed to 2.52 THz radiation.* Lasers in Surgery and Medicine, 2011. **43**(2): p. 152–163.
121. Wilmink, G.J., *et al. Determination of death thresholds and identification of terahertz (THz)-specific gene expression signatures*. in *Optical Interactions with Tissues and Cells XXI*. 2010: SPIE. **7562**: pp. 75620K-75620K-8.
122. Dalzell, D.R., *et al. Damage thresholds for terahertz radiation*. in *Optical Interactions with Tissues and Cells XXI*. 2010: SPIE. **7562**: pp. 75620M-75620M-8.
123. Ward, J.S., *et al. Tunable broadband frequency-multiplied terahertz sources*. in *Infrared, Millimeter and Terahertz Waves, 2008. IRMMW-THz 2008. 33 rd International Conference on*. 2008.
124. Eisele, H., *480 GHz oscillator with an InP Gunn device.* Electronics Letters, 2010. **46**(6): p. 422–423.
125. Eisele, H. and R. Kamoua, *High-performance oscillators and power combiners with InP Gunn devices at 260–330 GHz.* Microwave and Wireless Components Letters, IEEE, 2006. **16**(5): p. 284–286.
126. Mukherjee, M., *et al.*, *GaN IMPATT diode: a photo-sensitive high power terahertz source.* Semiconductor Science and Technology, 2007. **22**(12): p. 1258–1267.
127. Mukherjee, M. and S.K. Roy, *Wide-Bandgap III-V nitride based avalanche transit-time diode in Terahertz regime: Studies on the effects of punch through on high frequency characteristics and series resistance of the device.* Current Applied Physics, 2010. **10**(2): p. 646–651.
128. Buniatyan, V.V., *et al.*, *Silicon carbide TUNNETT diodes.* Solid-State Electronics, 2004. **48**(9): p. 1569–1577.
129. Ryzhii, V., *Graphene tunneling transit-time terahertz oscillator based on electrically induced p–i–n junction.* Applied Physics Express, 2009. **2**(3): p. 034503.

130. Nishizawa, J., T. Kurabayashi, and H. Makabe, *706-GHz GaAs CW fundamental-mode TUNNETT diodes fabricated with molecular layer epitaxy.* Physica Status Solidi (c), 2008. **5**(9): p. 2802–2804.
131. Asada, M., *Resonant Tunneling Diodes for Sub-Terahertz and Terahertz Oscillators.* Jpn. J. Appl. Phys, 2008. **47**: p. 4375–4384.
132. Lee, Y.-S., *Principles of terahertz science and technology.* 1st ed. 2008, New York, NY: Springer.
133. Daniel, C., Bernard, Epsztein, *Backward travelling wave oscillators*. 1959, Csf: United States.
134. Rudolf, K., *Backward wave tube*. 1961, ENGLISH ELECTRIC VALVE CO LTD: United States.
135. Kompfner, R. and N.T. Williams, *Backward-Wave Tubes.* Proceedings of the IRE, 1953. **41**(11): p. 1602–1611.
136. Il'ina, S., Bakaushina GF, Gaĭduk VI, Khrapko AM, Zinov'eva NB., *Possible role of water in transmitting the effect of millimeter range radiation to biological objects.* Biofizik, 1979. **24**(3): p. 513.
137. Carr, G.L., *et al.*, *High-power terahertz radiation from relativistic electrons.* 2002. **420**(6912): p. 153–156.
138. Doria, A., *et al.*, *THz radiation studies on biological systems at the ENEA FEL facility.* Infrared Physics & Technology, 2004. **45**(5–6): p. 339–347.
139. Grosse, E., *THz radiation from free electron lasers and its potential for cell and tissue studies.* Phys Med Biol, 2002. **47**(21): p. 3755–60.
140. Berns, M., *et al.*, *Free electron laser irradiation at 200 microns affects DNA synthesis in living cells.* Proceedings of the National Academy of Sciences of the United States of America, 1990. **87**(7): p. 2810–2812.
141. Berns, M., *et al.*, *Free electron laser irradiation at 200 microns inhibits DNA synthesis in living cells.* Journal of Laser Applications, 1994. **6**(7): p. 165–169.
142. Berns, M.W. and W. Bewley, *Inhibition of nucleic acid synthesis in cells exposed to 200 micrometer radiation from the Free electron laser.* Photochemistry and Photobiology, 1987. **46**(2): p. 165–167.
143. Richards, P.L., *Bolometers for infrared and millimeter waves.* J. Applied Physics, 1994. **76**(1): p. 1–23.
144. Sizov, F., *THz Radiation Sensors.* Opto-electronics review 2010. **18**(1): p. 10–36.
145. Kleine-Ostmann, T., *et al. In vitro field exposition of skin cells between 100 GHz and 2.52 THz*. in *Infrared, Millimeter, and Terahertz Waves, 2009. IRMMW-THz 2009. 34th International Conference on*. 2009.
146. Pikov, V. and P.H. Siegel, *Thermal monitoring: Raman spectrometer system for remote measurement of cellular temperature on a microscopic scale.* IEEE Eng Med Biol Mag, 2010. **29**(1): p. 63–71.
147. Wilmink, G.J., *et al.*, *Quantitative investigation of the bioeffects associated with terahertz radiation.* Lasers in Surgery and Medicine, 2010. **7562**(1): p. 75620L.
148. Kristensen, T., *et al.*, *Modeling terahertz heating effects on water.* Opt Express, 2010. **18**(5): p. 4727–39.
149. Gallerano, G.P. *THz-Bridge: Tera-Hertz radiation in Biological Research, Investigation on Diagnostics and study of potential Genotoxic Effects*. 2004 [cited 2009; Available from: http://www.frascati.enea.it/THz-BRIDGE/.
150. Jastrow, C., T. Kleine-Ostmann, and T. Schrader, *Numerical dosimetric calculations for in vitro field expositions in the THz frequency range.* Adv. Radio Sci., 2010. **8**: p. 1–5.
151. Ostrovskiy, N.V., *et al. Application of the terahertz waves in therapy of burn wounds*. in *Infrared and Millimeter Waves and 13th International Conference on Terahertz Electronics, 2005. IRMMW-THz* 2005.
152. Kirichuck, V., *et al.*, *Sex-specific differences in changes of disturbed functional activity of platelets in albino rats under the effect of terahertz electromagnetic radiation at nitric oxide frequencies.* Bulletin of Experimental Biology and Medicine, 2008. **145**(1): p. 75–77.
153. Kirichuk, V., Efimova, N., & Andronov, E.. , *Effect of High Power Terahertz Irradiation on Platelet Aggregation and Behavioral Reactions of Albino Rats.* Bulletin of Experimental Biology and Medicine, 2009. **148**(5): p. 746–9.
154. Kirichuk, V. and A. Tsymbal, *Effects of Terahertz Irradiation at Nitric Oxide Frequencies on Intensity of Lipoperoxidation and Antioxidant Properties of the Blood under Stress Conditions.* Bulletin of Experimental Biology and Medicine, 2009. **148**(2): p. 200–3.
155. Kirichuk, V. and A. Tsymbal, *Use of Terahertz Electromagnetic Waves for Correcting Hemostasis Functions.* Biomedical Engineering, 2010. **44**(1): p. 11–14.
156. Bondar, N., *et al.*, *Behavioral effect of terahertz waves in male mice.* Bulletin of Experimental Biology and Medicine, 2008. **145**(4): p. 401–405.
157. Zhengyu, M., *Biological research by optically pumped far infrared lasers.* Infrared Physics, 1989. **29**(2–4): p. 631–636.
158. Hu, N., *THz irradiation of d. melanogaster.* Applied infrared and optoelectronics, 1987. **1**: p. 7.
159. Federov, V., *Comparative study of the effects of infrared, submillimeter, and millimeter EM radiation.* Biophysics, 2001. **46**(2): p. 293–297.

160. Xiong, S. and P. Shaomin, *Influence of submillimeter laser radiation on the growth of paddy rice.* Applied Laser, 1986. **6**(33).
161. Peng, S., *Influence of submillimeter laser radiation on the growth of black beans.* Applied Laser, 1987. **7**(33): p. 169.
162. Xu, M. and S. Xiong, *FIR laser irradiation in wheat.* Applied infrared and optoelectronics 1988. **4**: p. 30.
163. He, Z.-P. and J.-W. Su, *Preliminary observation on the effect of submillimeter laser radiation on the somaclonal variation of rice.* Proc. China-Japan Symposium on Plant Biotechnology, 1988: p. 49–51.
164. Kirichuk, V., *et al.*, *Use of terahertz electromagnetic radiation for correction of blood rheology parameters in patients with unstable angina under conditions of treatment with isoket, an NO donor.* Bulletin of Experimental Biology and Medicine, 2008. **146**(3): p. 293–296.
165. Webb, S.J. and D.D. Dodds, *Inhibition of bacterial cell growth by 136 gc microwaves*. Nature, 1968. **218**(5139): p. 374–375.
166. Nishiyama, H. and J. Fujita, *A glycine-rich RNA-binding protein mediating cold-inducible suppression of mammalian cell growth.* Journal Cell Biology, 1997. **137**: p. 899–908.
167. Zalyubovskaya, N.P., *et al.*, *To biological activity of radiation in millimeter and submillimeter ranges.* Eksperimental'noy i Klinicheskoy Radiologii, 1970. **6**: p. 202–205.
168. Kiselev, V.K., Kuleshov E.M., Kamenev Yu.E., Delevsky Yu.P., Zarzhetskaya N.A., Makolinets V.I. , *Use of submillimeter laser technology in immunological studies.* Radiotekhnicheskie Systemy Millimetrovogo i Submillimetrovogo Diapazonov, 1991: p. 176–181.
169. Makolinets, V.I., *Influence of submillimeter wave radiation on some manifestation of immunoresponsives* Medithiskaya Reabilitologia, Kurortologiya i Fizioterapiya, 1996. **1**: p. 33–35.
170. Hadjiloucas, S., M. Chahal, and J. Bowen, *Preliminary results on the non-thermal effects of 200–350 GHz radiation on the growth rate of S. cerevisiae cells in microcolonies.* Physics in Medicine and Biology, 2002. **47**(21): p. 3831.
171. Federov, V., *Investigation of possibility of submillimeter laser using as instrument for diagnostics in medicine (Proceedings Paper).* SPIE 2007. **6734**(04): p. 1–7.
172. Bourne, N., *et al.*, *The effects of terahertz radiation on human keratinocyte primary cultures and neural cell cultures.* Altern Lab Anim, 2008. **36**(6): p. 667–84.
173. Federov, V., *Study of biological effects of electromagnetic radiation of submillimeter part of terahertz range.* Biomeditsiknskaya Radioelektronika, 2011.
174. Fedorov, V.I., *et al. Investigation of possibility of submillimeter laser using as instrument for diagnostics in medicine*. in *International Conference on Lasers, Applications, and Technologies 2007: Laser Technologies for Medicine*. 2007. Minsk, Belarus: SPIE.
175. Ramundo-Orlando, A., *et al.*, *Effect of low frequency, low amplitude magnetic fields onthe permeability of cationic liposomes entrapping carbonic anhydrase.* Bioelectromagnetics, 2000. **21**: p. 491–498.
176. Ramundo-Orlando, A., *Terahertz Radiation Effects and Biological Applications.* Journal of Infrared, Millimeter and Terahertz Waves, 2009. **30**(12): p. 1308–1318.
177. Bender, M., *et al.*, *Current status of cytogenetic procedures to detect and quantify previous exposures to radiation.* Mutation Research, 1988. **196**: p. 103–159.
178. Preston, R., J. San Sebastian, and A. McFee, *The in vitro human lymphocyte assay for assessing the clastogenicity of chemical agents.* Mutation Research, 1987. **189**: p. 175–183.
179. Vijayalaxmi and T. Prihoda, *Genetic damage in mammalian somatic cells exposed to radiofrequency radiation: A meta-analysis of data from 63 publications (1990–2005).* Radiation Research, 2008. **169**: p. 561–574.
180. Govorun, V.M., *et al.*, *Far-infrared radiation effect on the structure and properties of proteins.* International Journal of Infrared and Millimeter Waves, 1991. **12**(12): p. 1469–1474.
181. Fedorov, V.I., Pogodin A.S., Bespalov V.G., Putilin S.E., Smolyanskaya O.A., Grachev Ya.V., Kozlov S.A. , *Influence of pulsed overwide-range terahertz radiation on albumin conformation* Millimetrovye Volny v Biologii I Meditsine 2009. **2**: p. 50–58.
182. Wilmink, G.J., *et al.*, *Development of a compact terahertz time-domain spectrometer for the measurement of the optical properties of biological tissues.* Journal of Biomedical Optics, 2011. **16** (4): p. 047006-047010.
183. Nazarov, M., *et al.*, *Terahertz time-domain spectroscopy of biological tissues.* Quantum Electronics, 2008. **38**(7): p. 647.
184. Blackman, C.F., *et al.*, *Effects of nonionizing electromagnetic radiation on single cell biologic systems*. Annals of the New York Academy of Sciences, 1975. **247**(1): p. 352–366.